ARTICLE

https://doi.org/10.1038/s41586-018-0382-x

Creating a functional single-chromosome yeast

Yangyang Shao[1,2], Ning Lu[1,2], Zhenfang Wu[3], Chen Cai[2,3], Shanshan Wang[3], Ling-Li Zhang[2,3], Fan Zhou[4], Shijun Xiao[4], Lin Liu[4], Xiaofei Zeng[4], Huajun Zheng[5], Chen Yang[1], Zhihu Zhao[6], Guoping Zhao[1,5,7,8]*, Jin-Qiu Zhou[3]*, Xiaoli Xue[1]* & Zhongjun Qin[1]*

Eukaryotic genomes are generally organized in multiple chromosomes. Here we have created a functional single-chromosome yeast from a *Saccharomyces cerevisiae* haploid cell containing sixteen linear chromosomes, by successive end-to-end chromosome fusions and centromere deletions. The fusion of sixteen native linear chromosomes into a single chromosome results in marked changes to the global three-dimensional structure of the chromosome due to the loss of all centromere-associated inter-chromosomal interactions, most telomere-associated inter-chromosomal interactions and 67.4% of intra-chromosomal interactions. However, the single-chromosome and wild-type yeast cells have nearly identical transcriptome and similar phenome profiles. The giant single chromosome can support cell life, although this strain shows reduced growth across environments, competitiveness, gamete production and viability. This synthetic biology study demonstrates an approach to exploration of eukaryote evolution with respect to chromosome structure and function.

Almost all known natural eukaryotic species have multiple chromosomes, except for the male ant *Myrmecia pilosula*, which contains only one chromosome[1]. In addition, the number of chromosomes in eukaryotic species varies without a clear association with their biological characteristics. For instance, in mammals, human (*Homo sapiens*) diploid cells have forty-six chromosomes[2], whereas diploid cells of the Indian muntjac (*Muntiacus muntjak*) have the lowest number of chromosomes (six for the female and seven for the male)[3]. In fungi, haploid cells of the budding yeast *Saccharomyces cerevisiae* have sixteen chromosomes and a genome of approximately 12 Mb[4], whereas haploid cells of the fission yeast *Schizosaccharomyces pombe* have only three chromosomes and a genome of approximately 14 Mb[5]. The advantages to a eukaryotic cell of multiple chromosomes instead of a single one are not clear. In this study, we have reorganized the genome of the unicellular eukaryotic model organism *S. cerevisiae*, whose haploid cell contains sixteen chromosomes ranging from 230 to 1,500 kb[4], into one giant chromosome, in order to explore whether a yeast cell with an artificially fused single chromosome can survive and complete a sexual cycle.

Rationale

The creation of a single-chromosome yeast from *S. cerevisiae* BY4742 haploid cells required 15 rounds of chromosome end-to-end fusions, with deletion of 15 centromeres and 30 telomeres (Fig. 1a, Extended Data Table 1). During the fusion process, the following criteria and principles were followed. (1) To generate genetically stable fused chromosomes and avoid the formation of dicentric chromosomes[6], simultaneous deletions of one centromere and two telomeres in each round of fusion were required. We developed a method to precisely fuse two chromosomes by using both the efficient CRISPR–Cas9 cleavage system[7] and the robust homologous recombination activity of yeast (Fig. 1b). (2) The single centromere was intentionally kept roughly in the middle of the final single chromosome to maintain two arms with balanced lengths. (3) The order of chromosome fusion was randomly selected. Our pilot experiments showed that eight pairs of randomly selected chromosomes could all be successfully fused, and the resulting strains grew as robustly as the wild-type strain, indicating that the yeast cells could tolerate random fusion of two chromosomes. (4) The deleted regions of each centromere and telomere were carefully selected to avoid affecting adjacent genes. (5) In addition, the redundant copies of telomere-associated long repetitive sequences (over 2 kb; Extended Data Table 2) located on different chromosomes were deleted to avoid potential homologous recombination at undesired sites.

Chromosome fusion and confirmation

The first chromosome fusion strain, SY0, was constructed by simultaneously removing the telomere and telomere-associated long repetitive sequences of the right arm of chromosome VII (VIIR) and the left arm of chromosome VIII (VIIIL), as well as the centromere element in chromosome VIII (Fig. 1b). Following the same pair-wise fusion strategy, fourteen successive rounds of chromosome fusion were carried out in strain SY0, and finally strain SY14, with all sixteen chromosomes fused into one giant single linear chromosome, was successfully constructed (Extended Data Table 1). For each round of chromosome fusion, the positive rates confirmed by PCR sequencing ranged from 20 to 100% (Extended Data Table 1).

To validate the series of chromosome fusions in strains SY0–SY14, we examined the chromosome numbers using pulsed-field gel electrophoresis (PFGE) under various optimal conditions (Fig. 2a). With the accumulation of chromosome fusions, the DNA bands corresponding to the native chromosomes disappeared accordingly in the lower parts of the gels, and the DNA bands corresponding to the newly fused, larger chromosomes (indicated with red arrowheads) appeared in the upper parts of the gels. The single linear chromosome of SY14 (11.8 Mb) migrated most slowly and remained at the top of the gel (Fig. 2a).

[1]Key Laboratory of Synthetic Biology, CAS Center for Excellence in Molecular Plant Sciences, Shanghai Institute of Plant Physiology and Ecology, Chinese Academy of Sciences, Shanghai, China. [2]University of Chinese Academy of Sciences, Beijing, China. [3]The State Key Laboratory of Molecular Biology, CAS Center for Excellence in Molecular Cell Science, Shanghai Institute of Biochemistry and Cell Biology, Chinese Academy of Sciences, Shanghai, China. [4]Frasergen Bioinformatics Co., Ltd, Wuhan, China. [5]Shanghai-MOST Key Laboratory of Health and Disease Genomics, Chinese National Human Genome Center at Shanghai, Shanghai, China. [6]Beijing Institute of Biotechnology, Beijing, China. [7]Department of Microbiology and Li Ka Shing Institute of Health Sciences, The Chinese University of Hong Kong, Prince of Wales Hospital, Shatin, New Territories, Hong Kong SAR, China. [8]State Key Laboratory of Genetic Engineering, Department of Microbiology, School of Life Sciences and Institute of Biomedical Sciences, Fudan University, Shanghai, China. *e-mail: gpzhao@sibs.ac.cn; jqzhou@sibcb.ac.cn; xlxue@sibs.ac.cn; qin@sibs.ac.cn

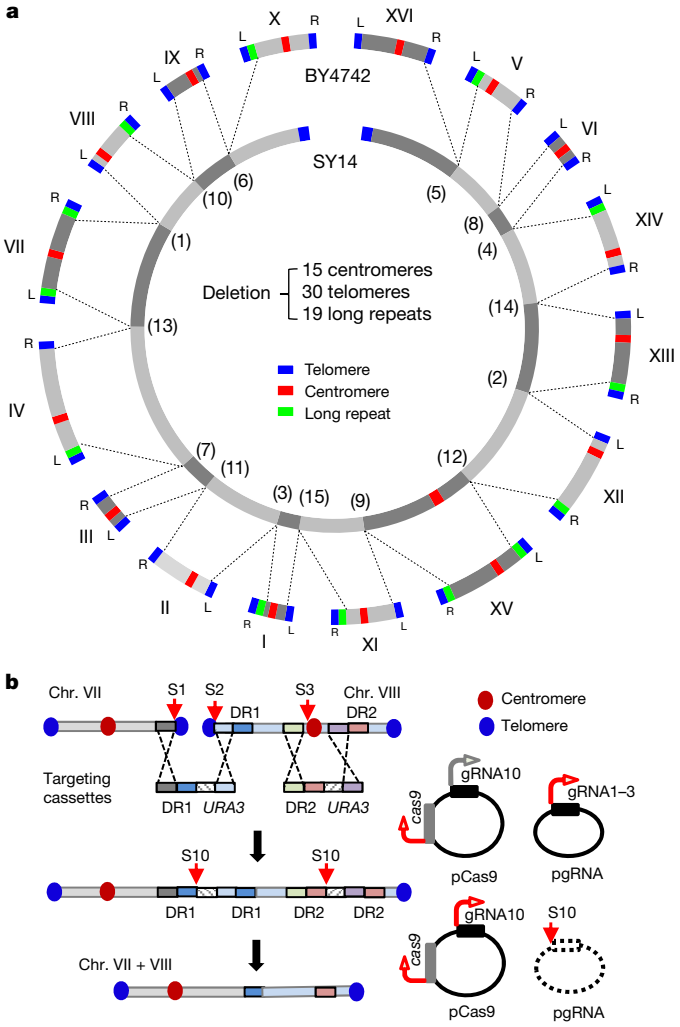

Fig. 1 | Creation of a single-chromosome yeast. a, Sixteen native chromosomes (I–XVI) of BY4742 (wild type) are aligned in the outer ring. The single chromosome of SY14 aligned in the inner ring has undergone fifteen sequential rounds of chromosomal end-to-end fusions, indicated by dashed lines. **b**, CRISPR–Cas9-mediated fusion of chromosomes VII and VIII. Cas9 nuclease cut at the telomere (sites S1 and S2) and centromere (site S3) loci with the guidance of gRNAs 1–3. The broken chromosomes were repaired through homologous recombination with the provided DNA targeting cassettes. The curation of *URA3* and the guide RNA expression plasmid (pgRNA) occurred simultaneously upon galactose induction.

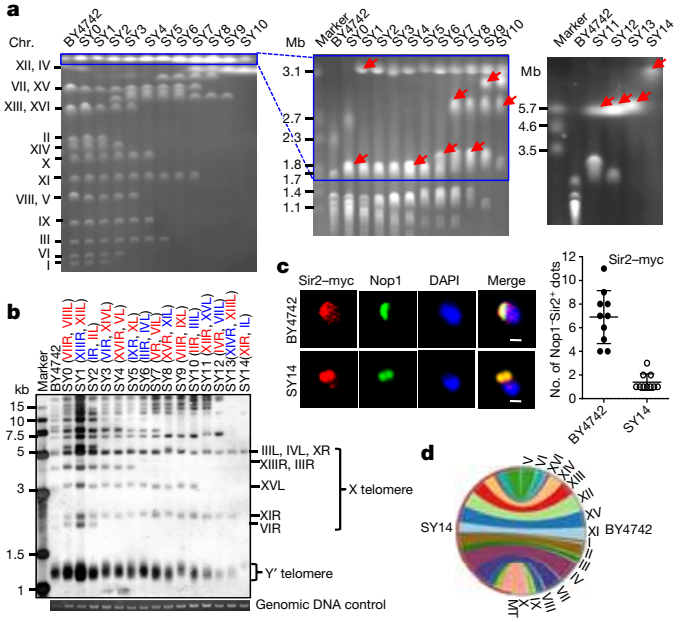

Fig. 2 | Confirmation of chromosome fusion(s) in yeast strains. a, Intact chromosomal DNA analysis by PFGE under different conditions. The red arrows indicate the newly fused chromosomes in each strain. Data shown are representative images of three independent experiment. **b**, The XhoI-digested genomic DNAs from the strains were Southern blotted with a telomere-specific TG_{1-3} probe. The X element- and X-Y′-containing telomeres are indicated in blue and red, respectively, in parentheses. Results are representative of two independent experiments. **c**, The myc-tagged telomere binding protein Sir2 was detected with polyclonal anti-myc antibody and Cy3-conjugated (red) secondary antibody. Nop1, a nucleolar protein, was detected with a monoclonal anti-Nop1 antibody and Alexa 488-conjugated (green) secondary antibody. DNA was stained by DAPI (blue). Scale bar, 1 μm. Data represent mean ± s.d. ($n = 10$ sections per genotype from three independent experiments). **d**, Comparison of the genome sequences of BY4742 (right) and SY14 (left). MT, mitochondrial genome.

The sizes of all chromosomal DNA bands were in agreement with the theoretical calculated sizes (Extended Data Table 1). In addition to PFGE, we performed Southern hybridization with a specific telomeric DNA probe to further confirm the proper chromosome fusions. Following each round of chromosome fusions, the corresponding telomere signals disappeared owing to deletion of these telomere sequences (Fig. 2b, Extended Data Fig. 1). The reduction in telomere numbers in the SY14 strain was visualized by immunostaining of the 13-myc-tagged telomere-binding protein Sir2 using anti-myc antibody[8]. In BY4742 cells, 32 telomeres clustered at 6–8 foci in the nuclei (Fig. 2c), consistent with previous reports[9,10]. Only one or two telomere signals were detected in SY14 cells. Notably, nucleolar structures in the SY14 cells, which could be seen by Nop1 staining (Fig. 2c), remained intact, suggesting that chromosome fusions caused little change in the chromatin region of ribosomal DNA (rDNA) loci.

The genomic DNA of the SY14 strain and its parental strain BY4742 were completely sequenced by a combination of PacBio and Illumina sequencing with 426- and 320-fold coverage, respectively. Their chromosomal nucleotide sequences were de novo assembled into 1 and 16 contigs, respectively. The approximately 1.5-Mb array of rDNA repeats (approximately 9.1 kb)[11] was difficult to assemble, and only several copies of rDNA repeats were assembled in both the BY4742 and SY14 genomes. The complete nucleotide sequences of the single chromosome of SY14 were compared with the sixteen chromosomes of BY4742, which showed excellent co-linearity (Fig. 2d), confirming that the chromosome orderings and orientations were as designed. Sequence alignments of the BY4742 and SY14 chromosomes revealed that all 61 designed deletions (Extended Data Table 1) had been successfully achieved (Fig. 2d, Extended Data Fig. 2); however, 11 single-nucleotide polymorphisms (SNPs) and 7 insertions and deletions (indels) that arose during chromosome fusions were detected using next-generation sequencing and validated by the Sanger method (Extended Data Table 3).

Chromosomal 3D structures

Previous studies have documented the higher-order folding and spatial architecture of all sixteen chromosomes in *S. cerevisae* cells[12,13]. We carried out chromosome conformation capture (3C)-derived Hi-C assays on BY4742 and SY14 cells and on two intermediate strains—SY6 (containing nine chromsomes: seven fused and two native) and SY13 (containing only two fused large chromosomes) (Extended Data Table 1). The global chromosome interactions and average chromosome 3D architecture of the different fusion cells were analysed and compared with those of BY4742 cells[14,15].

The contact maps of BY4742, SY6, SY13 and SY14 cells clearly showed sixteen, nine, two and one independent, distinct intra-chromosomal interaction large square lattice structures, corresponding to the sixteen, nine, two and one individual chromosomes, respectively

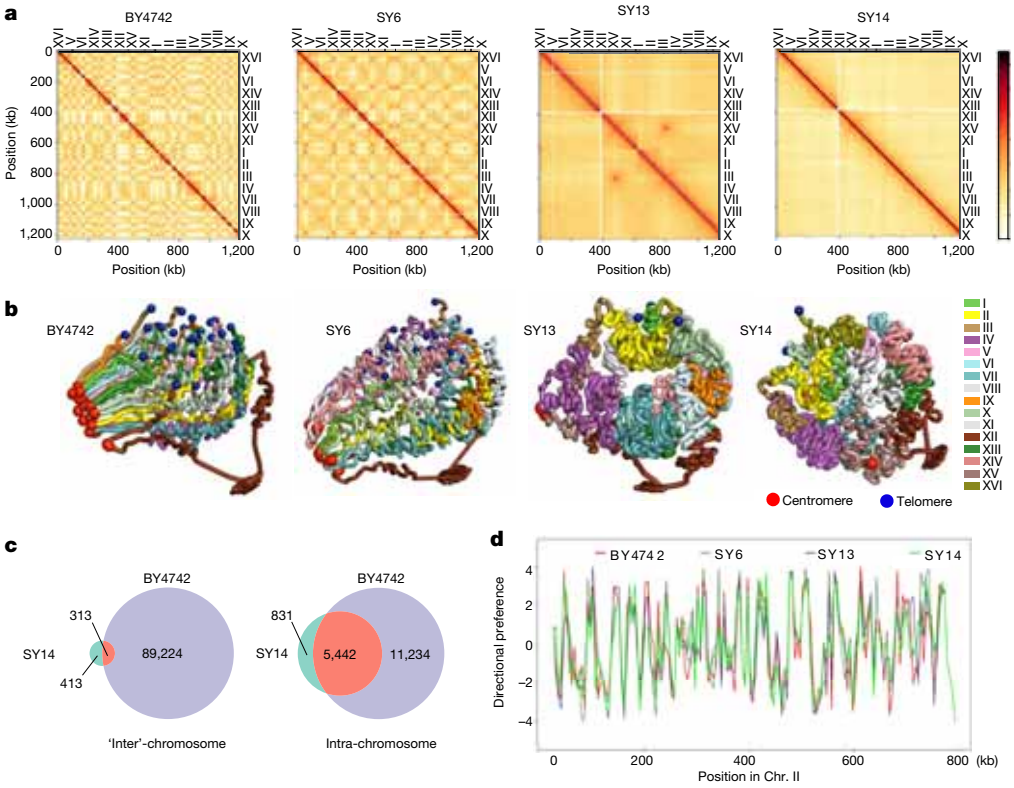

Fig. 3 | Chromosomal interactions and 3D structures of genomes in BY4742, SY6, SY13 and SY14 strains. a, The normalized contact heatmaps of four genomes with 10-kb resolution. Low to high interaction frequencies are depicted by a colour spectrum from light yellow to red. **b**, 3D conformations of the four genomes. **c**, Venn diagram for the numbers of significant ($P < 0.01$, $q < 0.01$) 'inter'- (left) and intra-chromosome (right) interactions. Note that intra- and 'inter'-chromosome here refer to locations in the BY4742 genome. **d**, The directional preferences of chromosome II from four genomes. A paired *t*-test[16] (*y*-axis) assessed the interaction preference of a specific genomic region (genomic coordinates with 5-kb bins shown in *x*-axis) against its upstream (negative *t*-value) or downstream (positive *t*-value) regions.

(Fig. 3a). The *Z*-score difference contact maps showed that the strong centromere–centromere interactions gradually disappeared along with the loss of corresponding centromeres (blue dots), but the interactions among the retained centromeres became much stronger (red dots) (Extended Data Fig. 3a). Consistent with a previous report[12], the sixteen chromosomes of BY4742 cells and the nine chromosomes of SY6 cells showed a typical Rabl configuration[12]: centromeres clustered around the spindle pole body, telomeres clustered with the nuclear envelope, and chromosome arms extending between these two anchoring points (Fig. 3b). Owing to the marked reduction in centromere and telomere numbers, the overall genome structures in SY13 and SY14 cells exhibited a relatively twisted, globular configuration with both the centromeres and telomeres located roughly on the periphery of the whole structure and the two arms of each chromosome much more bent than in BY4742 or SY6 cells, perhaps owing to the nuclear size limitation. It is worth noting that even in the case of the two chromosomes in SY13, the two centromeres and four telomeres were still clustered in roughly opposite positions in the nucleus, similar to the cases of BY4742 and SY6. Notably, the rDNA-repeat loci of all four strains were sequestered from the main structure (Fig. 3b). In particular, the substantial clustering of the flanking sequence of centromeres (red balls) and relative co-localization of the flanking sequence of telomeres (blue balls) in the BY4742 genome gradually disappeared as the chromosome fusion progressed from BY4742 to SY6, SY13 and SY14 (Fig. 3b). Notably, chromosomal fusion in SY6 caused little change to the configurations of the unfused chromosomes, such as chromosome XV, compared to those in BY4742 (Extended Data Fig. 4). However, with the accumulation of chromosome fusions, which resulted in a larger chromosome and a loss of the original centromeres, the 3D structures of chromosomes VI, XVI and X changed from stretched V shapes to more twisted globular shapes (Extended Data Fig. 4).

Almost all (97.8% and 99.7%) of the significant ($P < 0.01$, $q < 0.01$) inter-chromosomal interactions observed in BY4742 were absent in SY13 and SY14, respectively (Fig. 3c), probably owing to the elimination of most of the original centromeres and telomeres (Extended Data Fig. 3a, b). On the other hand, chromosome fusions brought two chromosomes that were distal from each other in BY4742 cells into close proximity, resulting in new significant ($P < 0.01$, $q < 0.01$) inter-chromosomal interactions; for example, the interaction between chromosomes XV and IV in SY13 cells, and chromosomes XV and XII in SY14 cells (Extended Data Fig. 3c). There were ten residual interactions of the single chromosome XV centromere region and chromosome II in all four strains, but the 3D structures of chromosomes XV and II did not show any possible spatial interactions between their centromere regions (Extended Data Fig. 3d). Unlike inter-chromosomal interactions, only 67.4% of total intra-chromosomal interactions were lost in the SY14 genome (Fig. 3c). In fact, the global direction preference[16], which quantifies the preference of a specific genomic region against its upstream or downstream interaction, was similar among BY4742, SY6, SY13 and SY14 cells for each chromosome (Fig. 3d, Extended Data Fig. 5), and the correlation coefficient was 0.90 ($P < 2.2 \times 10^{-16}$). This result strongly indicated that the local chromatin interactions of all the four strains, at least at the level of gene loci (as shown by the bin = 5 kb direction preference plot), were very similar.

Transcriptome and phenome analysis

The transcriptome profiles of the BY4742 and SY14 strains were analysed to evaluate the effects of changes in chromosome interactions and structure on global gene expression. Unexpectedly, the transcriptome of SY14 cells was nearly identical to that of BY4742 cells (Fig. 4a). Only 28 genes were differentially expressed in SY14 compared to BY4742 cells (Fig. 4b, Extended Data Table 4), accounting for 0.5% of the 5,815 protein-coding genes[4,17]. Fusion of all sixteen chromosomes into one repositioned the original telomere-adjacent genes to loci distal from telomeres, which presumably resulted in loss of the telomere position effect (TPE) and de-repression of these genes[18,19]. Accordingly, seven genes (*YFR057W*, *MAL11*, *THI5*, *YOL163W*, *YOL162W*, *SEO1* and *VTH1*) adjacent to the corresponding deleted telomeres were upregulated in SY14 cells. Notably, five genes (*ERR2*, *HSP32*, *FEX2*, *YPL277C* and *MPH3*) near the retained telomeres (XVI-L and X-R) in SY14 cells were downregulated, indicating an increase in the TPE. As about half of subtelomeric genes were deleted during chromosome fusions, the number of TPE-affected genes is likely to be underestimated in

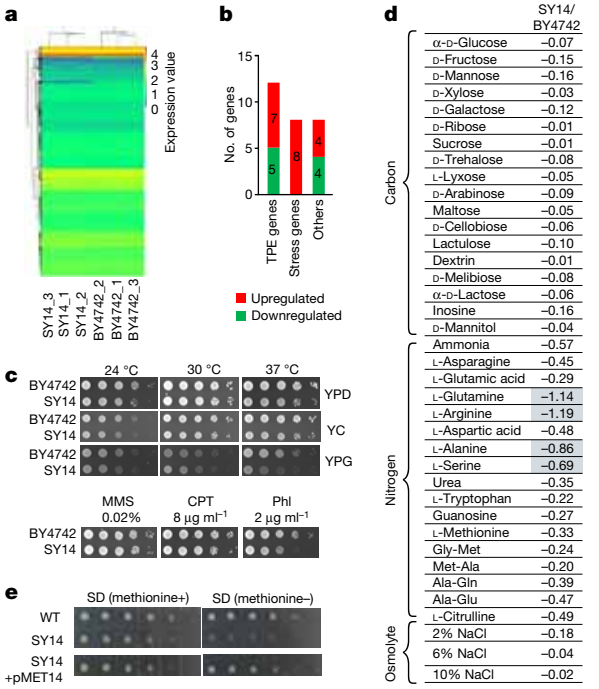

Fig. 4 | Transcriptome and phenome analyses. a, Heatmap of the transcriptome profiles of BY4742 and SY14 cells. The Pearson correlations ($n = 3$) are greater than 0.98 within each group and greater than 0.97 between different groups. **b**, Classification of differentially expressed genes, defined as those with $\log_2$(fold change) ≥ 1 and $P < 0.001$ in SY14 compared to wild-type cells. **c**, Fitness analysis of SY14 cells under various growth conditions. Representative results of two independent experiments. **d**, Growth comparison of BY4742 and SY14 cells under various conditions. The mean area of growth kinetics of SY14 cells from two independent experiments was normalized to those of BY4742 cells, and the numerical value of its logarithm base 2 is shown. The grey shaded negative values indicate greater than 50% growth reduction in SY14 cells. **e**, Restored growth of SY14 cells on medium without methionine by complementation of a functional *MET14* gene. SD, synthetic dextrose. Data are representative of three independent experiments.

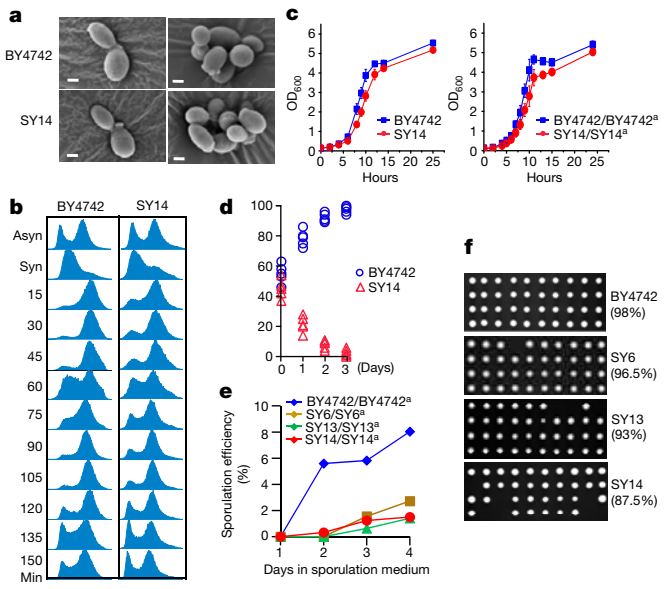

Fig. 5 | Sporulation and competition fitness. a, Scanning electron micrographs of BY4742 and SY14 cells. Scale bar, 1 μm. Representative images of three independent experiments. **b**, Cell cycle analysis. The yeast cells were synchronized with hydroxyurea and the progression of the cell cycle was analysed by flow cytometry. Data are representative of three independent experiments. **c**, Growth curves of the SY14 haploid (left) and diploid (right) strains (mean ± s.e.m.). Three biological replicates were assayed. **d**, Growth competition of BY4742 and SY14 haploid cells. Data from five biological replicates. **e**, Sporulation efficiency of diploid cells with different chromosome numbers. For each genotype, two independent diploid colonies were examined, and the results shared the same trend. **f**, Spore viability of tetrads. Spores of ten tetrads are shown. The spore viability was calculated from 60 tetrads for each strain. Data are representative of two independent experiments.

SY14 cells. Notably, eight genes involved in stress responses (especially DNA replication) were upregulated in SY14, suggesting that a giant single chromosome might introduce a new burden for chromosomal replication.

The SY14 cells demonstrated a slight reduction in growth fitness on complete media such as yeast extract peptone dextrose (YPD), yeast complete (YC) or YPG (similar to YPD but with glycerol as a carbon source), and an increased sensitivity to the genotoxic chemical phleomycin (Phl), but not methyl methanesulfonate (MMS) or camptothecin (CPT) (Fig. 4c). Phenotype microarray analysis showed that SY14 and BY4742 cells had comparable growth under conditions including different carbon sources and osmolytes, but SY14 cells showed a modest growth reduction under some nitrogen sources (Fig. 4d). We found that the expression of the *MET14* gene, which encodes an adenylyl-sulfate kinase, was reduced in SY14 cells comparing to the wild type ($\log_2$ fold-change $= -1.56$, $P = 5.97 \times 10^{-5}$; Extended Data Table 4). When a plasmid-borne *MET14* gene was introduced into SY14 cells, their growth on medium without methionine was restored (Fig. 4e), suggesting that deletion of the chromosome XI centromere accidently damaged the centromere-proximal promoter of *MET14*.

The size and shape of BY4742 and SY14 cells were similar (Fig. 5a). The pattern of cell cycle progression of SY14 cells resembled that of BY4742 cells (Fig. 5b), but the SY14 strain showed a slightly reduced growth rate (Fig. 5c). To evaluate whether the single-chromosome yeast could compete with the multi-chromosome yeast, we co-cultured SY14 and BY4742 cells and monitored their growth. As co-culture time increased, the number of SY14 haploid cells dropped rapidly, while the BY4742 haploid cells dominated the populations (Fig. 5d), suggesting that the competition fitness of the single-chromosome yeast is lower.

Meiosis and spore viability

Organisms that reproduce sexually are thought to have advantages over organisms that reproduce asexually. We evaluated the ability of the single-chromosome haploid cells to mate and form diploid cells and reproduce sexually. We constructed strains BY4742^a and SY14^a, in which the Matα cassette was replaced with a Mata cassette[20]. Haploid SY14 and SY14^a cells were able to mate to produce diploid cells, similarly to the parental strains. But the SY14/SY14^a cells displayed a slightly reduced growth rate (Fig. 5c). In addition, we noticed that two out of six colonies of SY14/SY14^a diploid cells could not maintain a correct diploid chromosome number upon mitotic division. Moreover, the SY14/SY14^a cells displayed weak competitiveness when co-cultured with BY4742/BY4742^a cells, and we observed the emergence of cells that contained genomes from both diploid cells (Extended Data Fig. 6a–c), indicating fusion of SY14/SY14^a and BY4742/BY4742^a cells.

The SY14/SY14^a cells were able to undergo meiosis to produce viable spores, but with reduced gamete production (Fig. 5e). In addition, the spore viability for SY14/SY14^a cells was 87.5%, which was lower than the 98% observed for BY4742/BY4742^a cells (Fig. 5f). The diploid cells of intermediate strains SY6/SY6^a and SY13/SY13^a displayed 96.5% and 93% spore viability, respectively (Fig. 5f), suggesting that spore viability is decreased as the number of chromosome fusions increases.

Discussion

Recently, synthetic biology has made great advances in the design and synthesis of individual chromosomes in the eukaryote *S. cerevisiae*. The synthesized cells largely resemble the wild-type cells[13,21], implying that this organism can tolerate large-scale genome engineering

well. In this study, we created a biologically functional *S. cerevisiae* (SY14) with a single giant chromosome by successive fusion of sixteen native chromosomes, representing, to our knowledge, the first example of a eukaryote with a single linear chromosome created in the laboratory.

Previous studies have suggested that the localization of a chromosome in the nucleus and inter-chromosome interactions affect gene expression[22,23]. In our study, chromosomal fusions involving sixteen chromosomes result in a loss of the majority of the inter-chromosomal interactions seen in parental cells, leading to marked changes in the overall chromosomal 3D structure. However, the global directional preferences at the level of gene loci (5-kb intervals) are largely retained in the SY14 cells. Accordingly, the transcriptome of the single-chromosome SY14 cells is nearly identical to that of the parental BY4742 cells. These observations demonstrate that inter-chromosomal interactions have a negligible effect on global gene transcription in yeast.

It was unexpected that the single point centromere in *S. cerevisiae*, which is only 125-bp long[24], can support the segregation and partition of the 11.8-Mb chromosome, which is eight times larger than the longest native chromosome. Nevertheless, several genes involved in the stress response, especially DNA replication stress, are upregulated in the single-chromosome yeast, consistent with the reported study of an increase in replication-induced topological stress with chromosome length in *S. cerevisiae*[25]. The tendency of SY14/SY14^{a} diploid cells to form polyploidy also suggests a functional defect of chromosome segregation in single-chromosome yeast; this is likely to cause the reduction in gamete production and viability in meiosis. Consistently, both the haploid and diploid cells of the single-chromosome yeast are disadvantaged when competing with wild-type cells. Therefore, the deleterious functional impact of a single giant chromosome, which may be due to chromosome replication and segregation, might explain why eukaryotic genomes are organized into multiple chromosomes. In fact, *S. cerevisiae* and its wild relative species have all maintained sixteen chromosomes across 10–20 million years of evolution, although their chromosome structures are not identical[26]. In an accompanying paper, another group created a two-chromosome budding yeast[27]. Their results are consistent with ours in that the chromosome fusions have minimal effects on cell growth and the transcriptome.

This study provides an alternative approach for studying the evolution of eukaryotes with respect to their chromosome structure and function. The series of strains (SY0–SY14) with successive fusions of sixteen chromosomes created in this study would be of considerable value for future investigations of telomere biology, centromere and kinetochore biology, meiotic recombination, and the relationship between nuclear organization and function.

Online content

Any Methods, including any statements of data availability and Nature Research reporting summaries, along with any additional references and Source Data files, are available in the online version of the paper at https://doi.org/10.1038/s41586-018-0382-x.

Received: 29 September 2017; Accepted: 22 June 2018;
Published online 1 August 2018.

1. Crosland, M. W. & Crozier, R. H. *Myrmecia pilosula*, an ant with only one pair of chromosomes. *Science* **231**, 1278 (1986).
2. Green, E. D., Watson, J. D. & Collins, F. S. Human Genome Project: Twenty-five years of big biology. *Nature* **526**, 29–31 (2015).
3. Lee, J. Y. et al. Simple purification of human chromosomes to homogeneity using muntjac hybrid cells. *Nat. Genet.* **7**, 29–33 (1994).
4. Goffeau, A. et al. Life with 6000 genes. *Science* **274**, 546–567 (1996).
5. Wood, V. et al. The genome sequence of *Schizosaccharomyces pombe*. *Nature* **415**, 871–880 (2002).
6. McClintock, B. The stability of broken ends of chromosomes in *Zea mays*. *Genetics* **26**, 234–282 (1941).
7. DiCarlo, J. E. et al. Genome engineering in *Saccharomyces cerevisiae* using CRISPR-Cas systems. *Nucleic Acids Res.* **41**, 4336–4343 (2013).
8. Moretti, P., Freeman, K., Coodly, L. & Shore, D. Evidence that a complex of SIR proteins interacts with the silencer and telomere-binding protein RAP1. *Genes Dev.* **8**, 2257–2269 (1994).
9. Gotta, M. et al. The clustering of telomeres and colocalization with Rap1, Sir3, and Sir4 proteins in wild-type *Saccharomyces cerevisiae*. *J. Cell Biol.* **134**, 1349–1363 (1996).
10. Zhou, J., Zhou, B. O., Lenzmeier, B. A. & Zhou, J. Q. Histone deacetylase Rpd3 antagonizes Sir2-dependent silent chromatin propagation. *Nucleic Acids Res.* **37**, 3699–3713 (2009).
11. Zhang, W. et al. Engineering the ribosomal DNA in a megabase synthetic chromosome. *Science* **355**, eaaf3981 (2017).
12. Duan, Z. et al. A three-dimensional model of the yeast genome. *Nature* **465**, 363–367 (2010).
13. Mercy, G. et al. 3D organization of synthetic and scrambled chromosomes. *Science* **355**, eaaf4597 (2017).
14. Dekker, J., Rippe, K., Dekker, M. & Kleckner, N. Capturing chromosome conformation. *Science* **295**, 1306–1311 (2002).
15. van Berkum, N. L. et al. Hi-C: a method to study the three-dimensional architecture of genomes. *J. Vis. Exp.* **39**, 1869 (2010).
16. Le, T. B., Imakaev, M. V., Mirny, L. A. & Laub, M. T. High-resolution mapping of the spatial organization of a bacterial chromosome. *Science* **342**, 731–734 (2013).
17. Engel, S. R. et al. The reference genome sequence of *Saccharomyces cerevisiae*: then and now. *G3 (Bethesda)* **4**, 389–398 (2014).
18. Wellinger, R. J. & Zakian, V. A. Everything you ever wanted to know about *Saccharomyces cerevisiae* telomeres: beginning to end. *Genetics* **191**, 1073–1105 (2012).
19. Mitchell, L. A. & Boeke, J. D. Circular permutation of a synthetic eukaryotic chromosome with the telomerator. *Proc. Natl Acad. Sci. USA* **111**, 17003–17010 (2014).
20. Xie, Z. X. et al. Rapid and efficient CRISPR/Cas9-based mating-type switching of *Saccharomyces cerevisiae*. *G3 (Bethesda)* **8**, 173–183 (2018).
21. Richardson, S. M. et al. Design of a synthetic yeast genome. *Science* **355**, 1040–1044 (2017).
22. Spilianakis, C. G., Lalioti, M. D., Town, T., Lee, G. R. & Flavell, R. A. Interchromosomal associations between alternatively expressed loci. *Nature* **435**, 637–645 (2005).
23. Cremer, T. & Cremer, M. Chromosome territories. *Cold Spring Harb. Perspect. Biol.* **2**, a003889 (2010).
24. Verdaasdonk, J. S. & Bloom, K. Centromeres: unique chromatin structures that drive chromosome segregation. *Nat. Rev. Mol. Cell Biol.* **12**, 320–332 (2011).
25. Kegel, A. et al. Chromosome length influences replication-induced topological stress. *Nature* **471**, 392–396 (2011).
26. Yue, J. X. et al. Contrasting evolutionary genome dynamics between domesticated and wild yeasts. *Nat. Genet.* **49**, 913–924 (2017).
27. Luo, J., Sun, X., Cormack, B. P. & Boeke, J. D. Karyotype engineering by chromosome fusion leads to reproductive isolation in yeast. *Nature* https://doi.org/10.1038/s41586-018-0374-x (2018).

Acknowledgements We thank X. Gao, W. Zhao, and J. Li for technical help. This research was supported by the Strategic Priority Research Program of the Chinese Academy of Sciences (XDB19000000), the National Natural Science Foundation of China (31421061, 31770099, 31370120, 31230040), the National Key Basic Research Program of China (973 Program) (2011CBA00801, 2012CB721102), and the National Key Research and Development Program of China (2016YFA0500701).

Reviewer information *Nature* thanks G. Liti, K. Wolfe and the other anonymous reviewer(s) for their contribution to the peer review of this work.

Author contributions Z.Q. and X.X. designed and analysed all experiments. J.-Q.Z. and G.Z. contributed to the experiment designs and data evaluation. Y.S. constructed the single-chromosome yeast and conducted the scanning electron microscopy characterization. N.L. conducted the PFGE confirmation, growth characterization and cell cycle experiments. C.C. and L.-L.Z. conducted meiosis and genotoxin sensitivity experiments. Z.W. and S.W. conducted telomere characterization. S.X., X.Z. and H.Z. performed genome analysis. Z.Z. designed the Hi-C and part of the RNA-seq experiments and data interpretation. F.Z., L.L. and Z.Z. performed chromosome Hi-C data analysis. F.Z. analysed the RNA-seq data. X.X. and C.Y. analysed the phenotype microarray data. X.X. wrote the primary manuscript with contributions from J.-Q.Z., Z.Q., G.Z., Z.Z., C.Y., S.X. and Z.W.

Competing interests The authors declare no competing interests.

Additional information
Extended data is available for this paper at https://doi.org/10.1038/s41586-018-0382-x.
Supplementary information is available for this paper at https://doi.org/10.1038/s41586-018-0382-x.
Reprints and permissions information is available at http://www.nature.com/reprints.
Correspondence and requests for materials should be addressed to G.Z. or J.-Q.Z. or X.X. or Z.Q.
Publisher's note: Springer Nature remains neutral with regard to jurisdictional claims in published maps and institutional affiliations.

METHODS

No statistical methods were used to predetermine sample size. The experiments were not randomized and the investigators were not blinded to allocation during experiments and outcome assessment.

Plasmid constructions. The Cas9 expression plasmid pCas9 was constructed from pMetCas9[28] by replacing the selection marker *MET14* with *LEU2*. The guide RNA expression plasmid (pgRNA) was constructed in three steps: (1) the vector pHIS426 was constructed by Gibson assembly[29] of the *HIS3* gene amplified from *S. cerevisae* S288C genomic DNA and vector backbones amplified from p426-SNR52p-gRNA.CAN1.Y-SUP4t. (2) Each guide RNA expression cassette contains the *SNR52* promoter, a 20-bp target sequence and the structural component of guide RNA, followed by the SUP 3′ flanking sequence. The 20-bp target sequences of guide RNAs 1, 2 and 3 were manually selected from the upstream of any 5′-NGG near the to-be-deleted centromere and telomeres. The guide-RNA expression cassettes were generated by fusion PCR of two segments, the SNR52 promoter and the guide RNA structural component/the SUP 3′ flanking sequence segment, both of which were PCR amplified using p426-SNR52p-gRNA.CAN1.Y-SUP4t (Addgene plasmid ID: 43803) as a template. For each guide RNA expression cassette, a 20-bp RNA target sequence and specific restriction sites were introduced at the 5′ end of PCR primers. (3) The three target cassettes gRNA1, gRNA2 and gRNA3 were digested with pairs of restriction enzymes EcoRI–BamHI, BamHI–NcoI and NcoI–NotI, respectively, and were ligated to an EcoRI–NotI-digested pHIS426.

CRISPR–Cas9 facilitated chromosome fusion. Approximately 1 μg of each DNA targeting cassette (with 50–400 bp homology arms and 200 bp direct repeat (DR) sequences for the curation of selection markers in the second step) and pgRNA were co-transformed in *S. cerevisae* BY4742 (Euroscarf, not tested for mycoplasma) cells harbouring pCas9, which constitutively expressed Cas9, using a standard lithium acetate transformation protocol[30]. The transformation products were plated on the synthetic drop-out medium SC-Ura-His-Leu (omitting uracil, histidine and leucine). The positive colonies verified by PCR sequencing were inoculated and grown in 3 ml of SC-Ura-His-Leu liquid medium to saturation at 30 °C. The cell cultures were then transferred to SC-Leu medium containing 2% galactose and 3% raffinose instead of 2% glucose, with an initial optical density of $OD_{600} = 0.3$. After 16 h, 100 μl of culture was plated and grown on SC-Leu with 1 mg/ml 5-FOA. The curation of selection markers and pgRNA of the positive colonies was verified by PCR analysis and sequencing. The verified single colony was inoculated in SC-Leu medium to start the next round of chromosome end-to-end fusion.

Telomere Southern blot. Telomere Southern blotting and hybridization were performed as previously described[31]. In brief, roughly equal amounts of genomic DNA were digested with XhoI, and separated by electrophoresis on 1.0% agarose gel. The DNA was then transferred to a Hybond-N+ Nylon membrane (GE Healthcare). Probe labelling, hybridization and immunological detection were performed using DIG-High Prime DNA Labelling and the Detection Starter Kit II (Roche). An 81-bp TG_{1-3} DNA fragment was chosen as a telomere-specific probe, and a fragment from chromosome I served as a non-telomeric control probe.

Genome sequencing, assembly and data accessibility. A total of 20 μg of high quality genome DNA was extracted from BY4742 and SY14 cells. A 20 kb SMRT-bell sequencing library (Pacific Biosciences) was constructed using a size selection protocol on the BluePippin (Sage Science). The two SMRT-bell yeast genomic libraries were sequenced using 3 SMRT cells (Pacific Biosciences) with a 10-h moving time window in the PacBio Sequel (Pacific Biosciences) sequencing platform. Primary filtering on polymerase reads was performed using the SMRT analysis package V4.0 (https://www.pacb.com/support/software-downloads/).

To assemble the BY4742 and SY14 genomes, 320× and 426× of PacBio subreads were used, respectively. The genomic sequence data of SY14 and BY4742 genomes were directly assembled into 1 and 16 contigs using CANU[32] (version 1.5) without additional data or scaffolding steps. The assembled genomes have no Ns in their sequences. Owing to the high number of repeats in the rDNA region (100–200 copies[11] of ~9,100 bp unit), we could not assemble all repeat sequences for this highly repeated region. Using longer reads of PacBio sequencing, we have assembled a repeated region longer than reported in the public S288C reference genome (GCF_000146045.2_R64/). The nuclear genomes were revised using pbalign (https://github.com/PacificBiosciences/pbalign, version 0.3.1, algorithm: blasr, hitPolicy: randombest, algorithmOptions:–bestn 1–nCandidates 1–bam, maxDivergence 15.0, minAccuracy 85.0) and arrow (https://github.com/PacificBiosciences/GenomicConsensus, version 2.2.0, minCoverage 15). The mitochondrial genomes of BY4742 and SY14 were assembled using minimap (version 0.2-r124-dirty) and miniasm (version 0.2-r137-dirty)[33]. The revision of mitochondrial genomes of BY4742 and SY14 cells was performed using the same procedure with modified parameters of max Divergence 30.0, min Accuracy 70.0 (pbalign) and min Coverage 30 (arrow). The mitochondrial genomes were cyclized with minimus2 (https://github.com/sanger-pathogens/circlator/wiki/Minimus2-circularization-pipeline, AMOS, version 3.1.0).

The genomes of BY4742 and SY14 cells were aligned using LAST[34] (version 810). The scripts last-split[34] and maf-swap were used to achieve 1-to-1 alignment according to the manual (http://last.cbrc.jp/doc/last-split.html). The alignments between two genomes were extracted from LAST output using a custom Python script and plotted with Circos[35] (version 0.67-7). To correct for possible error of Single Molecule Real-Time (SMRT) sequencing reads (predominantly either deletions or insertions) and to obtain the reliable genomic difference between BY4742 and SY14, we re-sequenced both SY14 and BY4742 whole genomes using next generation sequencing (NGS) Illumina pair-end sequencing, which provided 200× coverage for SY14 and 233× coverage for BY4742 cells. These new sequence data were mapped to the S288C genome to identify the genomic differences between the two strains, which were further validated by Sanger sequencing.

Hi-C library preparation and sequencing. The genomic DNA from exponential phase cells was cross-linked and digested with 200 unit MboI enzyme (NEB) as previously described[36]. The cutting DNA ends were labelled with biotin-14-dCTP (TriLINK) followed by ligation. Purified DNA was sheared to a length of ~400 bp. Point ligation junctions were pulled down with Dynabeads MyOne Streptavidin C1 (Thermofisher). The Hi-C library for Illumina sequencing was prepped with the NEBNext Ultra II DNA library Prep Kit for Illumina (NEB) according to the manufacturers' instructions. Fragments between 400 and 600 bp were paired-end sequenced on a HiSeq2000 platform (Illumina).

Construction of contact map and chromosome 3D model from Hi-C data. Using the ICE software package (version 1f8815d0cc9e)[37], the Hi-C data of BY4742 cells were iteratively mapped to the BY4742 genome, while the Hi-C data of SY6, SY13 and SY14 cells were mapped to their own genomes. Dandling ends and other unusable data were filtered, and the valid pairs were binned into 10-kb non-overlapping genomic intervals to generate contact maps. The contact maps were normalized using an iterative normalization method to eliminate systematic biases. To correct the overall decay of chromatin contacts with genomic distance, the whole genome interactions of BY4742 compared to SY6, SY13 and SY14 cells were transformed into *Z*-score using E. Crane's method[38] (package cworld-dekker from https://github.com/dekkerlab/cworld-dekker/releases, v1.01). Then, we calculated the difference between the *Z*-scores of SY14, SY13 and SY6 to BY4742 to infer the difference between their whole genome interactions. The chromosomal 3D structures of the four strains were inferred using the Pastis (v0.1) method[39] with a multidimensional scaling (MDS) model. The 10-kb contact maps were used to construct the 3D model. The rDNA region was reconstructed by assuming that every bin in rDNA loci was equally in contact with the remainder of the genome.

Calculation of intra-and inter-chromosome interactions. As the correlation efficiency of the two biological replicates for each strain was very high (>0.98) using QuASAR-Rep analysis (from HiFive[40] v1.5.3)[41], we pooled the data from two replicates together for significant interactions. The contacts between 5-kb pairs of intra-chromosome bins of four strains were transferred to Ay's Fit-Hi-C software (v1.0.1)[42] to calculate the corresponding cumulative probability *P* value and false discovery rate (FDR) *q* value[43]. After calculation, the interactions in which both the *P* value and *q* value were less than 0.01 were identified as significant interactions.

The statistical significance and false discovery rate of the inter-chromosome interactions of BY4742, SY6 and SY13 cells were calculated using Xie's method[44]. We then calculated the FDR *q* value, and the interactions in which both the *P* value and *q* value were less than 0.01 were identified as significant interactions.

Comparison of significant interactions. Interactions were considered significant at $P < 0.01$, $q < 0.01$.The coordinates of SY14, SY13 and SY6 genome bins were mapped to those in the BY4742 genome by sequence alignment. For better comparison, we separated the interactions into intra-chromosome and 'inter'-chromosome (between original chromosome regions) and performed pairwise comparison. We defined the sequences of 100 MboI-cutting sites around the centromere as the centromere regions, and the sequences of 100 MboI-cutting sites adjacent to the telomeres as the telomeres regions.

RNA-seq analysis. The BY4742 and SY14 cells from early-log phase ($OD_{600} = 1$) were collected, and their RNA was isolated using the TRIzol (Invitrogen) method[45]. The library preparation followed the standard procedure (BGI). The libraries were sequenced on the Illumina HiSeq 4000 platform using the 150-bp pair-end sequencing strategy. For each sample, 6 Gb of clean data was obtained. The cleaned reads were mapped onto the *S. cerevisiae* S288C reference genome (GCF_000146045.2_R64/) using Bowtie2 (v2.2.2)[46], and the abandon estimation was conducted by RSEM (v1.3.0)[47]. The significant differentially expressed genes (DEGs) were identified by DEseq2 (v1.16.1)[48] with definition of fold change more than 2 and false discovery rate (FDR) <0.001.

Phenotypic microarray analysis. Cells freshly grown on YPAD plates were inoculated into a yeast nutrient supplement mixture (NS × 48-0.48 mM L-histidine HCl, 4.8 mM L-leucine, 2.4 mM L-lysine HCl, and 1.44 mM uracil) and adjusted to a transmittance of 62% T using a Biolog turbidimeter (Biolog). Phenotypic microarray plates PM1–PM10 (Biolog) coated with different nutrients and chemical substrates

were used to incubate three cell types. For PM1-8, Biolog growth medium was prepared using IFY-0 (IFY-0 × 1.2) base inoculating fluid, supplemented with a mixture of 0.02% (v/v) yeast nutrient supplement mixture (NS × 48) and 0.013% (v/v) dye mix D (Biolog). To the growth medium, an extra 100 mM D-glucose had to be added for PM3-8. For PM9 and 10, Biolog growth medium was prepared using 0.67% (w/v) YNB w/o amino acids (Sunrise Science) and 0.12% (w/v) SC amino acid mixture (Sunrise Science) supplemented with a mixture of 0.01% (v/v) yeast nutrient supplement mixture (NS × 48), 0.01% (v/v) dye mix E (Biolog) and 100 mM D-glucose. The final volume of 12 ml was reached using reverse osmosis (RO) sterile water for every phenotypic microarray plates and added at 100 μl/well. Data were recorded photographically at 15 min intervals at 30 °C for 120 h and converted to a value reflecting metabolic activity by the OmniLog software (version 2.3.01).

Cell growth, morphology and cell cycle analysis. Strains BY4742 and SY14 were freshly streaked on plates, and three individual colonies were picked and inoculated in liquid YPAD medium overnight at 30 °C. The cell cultures were harvested and diluted in 25 ml of fresh liquid YPAD medium to a final OD_{600} of ~0.1. The optical density of cells was measured hourly and exponentially growing cells were collected. The samples were prepared for scanning electron microscopy (Zeiss) as described previously[49].

Methods of cell synchronization and cell cycle analysis using flow cytometry (Beckman) were performed as previously described[50]. In brief, the yeast strains were synchronized with 200 mM hydroxyurea for 1.5 h. Then, cells were washed five times with pre-warmed YPAD for release from hydroxyurea. The cells were collected every 15 min, washed, and fixed in 70% ethanol at 4 °C overnight. Cells were then treated with RNase (20 mg/ml, Sigma) at 37 °C for 2–3 h. Samples were stained by PicoGreen (Invitrogen), and analysed by flow cytometry. Approximately, 10^5 cells were analysed for each strain. Data were analysed with Summit 5.2.

Genotoxin sensitivity assay. Single colonies of the tested strains were cultured in YPD medium at 30 °C overnight. The cell numbers were adjusted to about equal for each strain, and tenfold serial dilutions were spotted onto plates with or without the indicated genotoxins. The plates were photographed after incubation at 30 °C for 2 to 3 days. For temperature sensitivity assay, plates were incubated at 24 °C, 30 °C and 37 °C for 2 to 3 days before photography.

Growth competition. The *HIS3* and *URA3* genes were introduced into BY4742 and SY14 chromosomes, respectively. Approximately 1×10^4 exponentially grown cells of BY4742 and SY14 haploid cells were co-inoculated in fresh YPD medium at 30 °C. The co-cultures were diluted to 0.05% daily with fresh YPD. The co-cultures after 0, 1, 2 and 3 days were plated on YPD plates, and 100 colonies grown from these plates were spotted on both SC-His (synthetic complete medium without histidine) and SC-Ura (synthetic complete medium without uracil) plates to calculate the viable cells of BY4742 and SY14, respectively. The growth competition of BY4742/BY4742^a and SY14/SY14^a diploid cells were carried out similarly.

Immunofluorescence. A 13-myc epitope-tag sequence was inserted at the genomic locus of the *SIR2* gene. Indirect immunofluorescence was performed as described previously[10]. Cells were grown in YPD medium overnight to a density of 1–2 × 10^7 cells/ml and fixed for 30 min by incubation with 4% formaldehyde. Next, cells were washed with 0.1 M potassium phosphate (pH 6.5) and P solution (1.2 M sorbitol and 1 M K_2PO_4), and re-suspended in P solution. Cells were subsequently treated with 0.1 mg/ml zymolyase (20T, MP Biomedicals) for 10 min, washed with P solution, and spotted on poly-L-lysine pre-treated slides. After rinsing in PBS-T buffer (PBS containing 0.1% Triton X-100 and 1% BSA), slides were incubated overnight at 4 °C with anti-Myc, anti-Rap1 and anti-Nop1 antibody diluted in PBS containing 1% BSA. Slides were then washed with PBS-T buffer and incubated with the appropriate secondary antibodies conjugated to Cy3 or Alexa 488. The DNA fluorescence signal was detected by DAPI (1 μg/ml in phosphate buffered saline (PBS) solution) staining. Slides were mounted with PBS containing 1 mg/ml p-phenylenediamine, 2.5 μM NaOH, and 90% glycerol. Confocal microscopy (Leica) was performed on a Leica TCS SP2 microscope with a 63 × lambda blue objective (oil). Image processing included similar filtration and threshold level standardization for all images.

Switching the MATα mating-type of the SY14 strain to MATa to generate the SY14^a strain. Most sequence of the 'MATa' and 'MATα' loci in different mating type yeasts are identical except that a 703 bp region in the MATa locus (5′-cttgatttttgttctttcggggaa…tgtagagtggtttgacgaataatt-3′) is different from an 807 bp region in the MATα locus (5′-tatgtctagtatgctggatttaaa…gttgacgaataattatgctgaagt-3′). We used the CRISPR–Cas9 system to replace the 703 bp sequence with the 807 bp sequence in the BY4742 and SY14 strains, to generate BY4742^a and SY14^a strains, respectively.

Mating and sporulation assays. Mating of MATa and MATα strains was performed on YPD plates by micromanipulation. Colonies of the resulting diploid strains were re-streaked on a new YPD plate to obtain a single clone. The diploids were verified by PCR amplifications using the two pairs of primers specific for the different mating-type loci. For sporulation, diploid strains were inoculated into 5 ml of sporulation medium to a density of $OD_{600} = 0.6$ and cultivate the strains at 23 °C. Use hemocytometer to count a total of ≥ 200 cells every 24 h, and sporulation efficiency was measured by the ratio of the number of asci containing 3 or 4 spores to that of the unsporulated cells. Spores were dissected, and at least 60 tetrads were dissected to measure spore viabilities.

Reporting summary. Further information on experimental design is available in the Nature Research Reporting Summary linked to this paper.

Data Availability. Genome sequencing data and the assembled genome sequences of SY14 and WT have been submitted to NCBI with a project accession number of PRJNA429985. The Hi-C sequencing data of SY6, SY13, SY14 and BY4742 have been submitted to NCBI with a project accession number of PRJNA431161. The RNA-seq data have been submitted to NCBI with a project accession number of PRJNA451522. All data can be viewed in NODE (http://www.biosino.org/node) by pasting the accession (NODEP00371807) into the text search box or through the URL: http://www.biosino.org/node/project/detail/NODEP00371807.

28. Zhou, J., Wu, R., Xue, X. & Qin, Z. CasHRA (Cas9-facilitated Homologous Recombination Assembly) method of constructing megabase-sized DNA. *Nucleic Acids Res.* **44**, e124 (2016).
29. Gibson, D. G. et al. Enzymatic assembly of DNA molecules up to several hundred kilobases. *Nat. Methods* **6**, 343–345 (2009).
30. Gietz, R. D. & Schiestl, R. H. High-efficiency yeast transformation using the LiAc/SS carrier DNA/PEG method. *Nat. Protocols* **2**, 31–34 (2007).
31. Wu, Z. et al. Rad6-Bre1-mediated H2B ubiquitination regulates telomere replication by promoting telomere-end resection. *Nucleic Acids Res.* **45**, 3308–3322 (2017).
32. Koren, S. et al. Canu: scalable and accurate long-read assembly via adaptive *k*-mer weighting and repeat separation. *Genome Res.* **27**, 722–736 (2017).
33. Li, H. Minimap and miniasm: fast mapping and de novo assembly for noisy long sequences. *Bioinformatics* **32**, 2103–2110 (2016).
34. Frith, M. C. & Kawaguchi, R. Split-alignment of genomes finds orthologies more accurately. *Genome Biol.* **16**, 106 (2015).
35. Krzywinski, M. et al. Circos: an information aesthetic for comparative genomics. *Genome Res.* **19**, 1639–1645 (2009).
36. Lieberman-Aiden, E. et al. Comprehensive mapping of long-range interactions reveals folding principles of the human genome. *Science* **326**, 289–293 (2009).
37. Imakaev, M. et al. Iterative correction of Hi-C data reveals hallmarks of chromosome organization. *Nat. Methods* **9**, 999–1003 (2012).
38. Crane, E. et al. Condensin-driven remodelling of X chromosome topology during dosage compensation. *Nature* **523**, 240–244 (2015).
39. Varoquaux, N., Ay, F., Noble, W. S. & Vert, J. P. A statistical approach for inferring the 3D structure of the genome. *Bioinformatics* **30**, i26–i33 (2014).
40. Sauria, M. E., Phillips-Cremins, J. E., Corces, V. G. & Taylor, J. HiFive: a tool suite for easy and efficient HiC and 5C data analysis. *Genome Biol.* **16**, 237 (2015).
41. Yardimci, G. et al. Measuring the reproducibility and quality of Hi-C data. Preprint at https://www.biorxiv.org/content/early/2018/02/05/188755 (2017).
42. Ay, F., Bailey, T. L. & Noble, W. S. Statistical confidence estimation for Hi-C data reveals regulatory chromatin contacts. *Genome Res.* **24**, 999–1011 (2014).
43. Benjamini, Y. & Hochberg, Y. Controlling the false discovery rate: a practical and powerful approach to multiple testing. *J. R. Stat. Soc. B* **57**, 289–300 (1995).
44. Xie, T., Yang, Q.-Y., Wang, X.-T., McLysaght, A. & Zhang, H.-Y. Spatial colocalization of human ohnolog pairs acts to maintain dosage-balance. *Mol. Biol. Evol.* **33**, 2368–2375 (2016).
45. Gayral, P. et al. Next-generation sequencing of transcriptomes: a guide to RNA isolation in nonmodel animals. *Mol. Ecol. Resour.* **11**, 650–661 (2011).
46. Langmead, B. & Salzberg, S. L. Fast gapped-read alignment with Bowtie 2. *Nat. Methods* **9**, 357–359 (2012).
47. Li, B. & Dewey, C. N. RSEM: accurate transcript quantification from RNA-Seq data with or without a reference genome. *BMC Bioinformatics* **12**, 323 (2011).
48. Love, M. I., Huber, W. & Anders, S. Moderated estimation of fold change and dispersion for RNA-seq data with DESeq2. *Genome Biol.* **15**, 550 (2014).
49. Bennis, S., Chami, F., Chami, N., Bouchikhi, T. & Remmal, A. Surface alteration of *Saccharomyces cerevisiae* induced by thymol and eugenol. *Lett. Appl. Microbiol.* **38**, 454–458 (2004).
50. Manukyan, A., Abraham, L., Dungrawala, H. & Schneider, B. L. Synchronization of yeast. *Methods Mol. Biol.* **761**, 173–200 (2011).

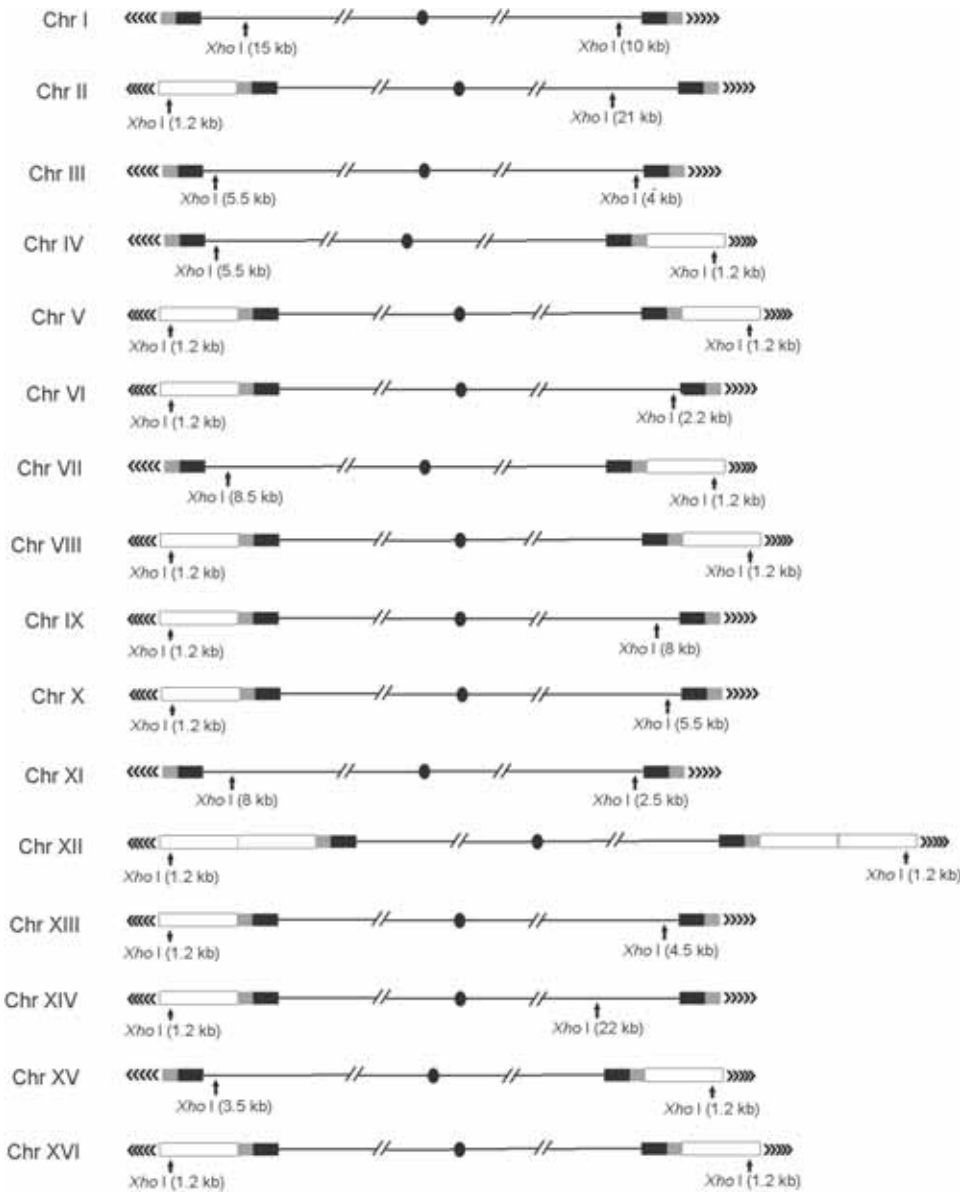

Extended Data Fig. 1 | Theoretical XhoI digestion pattern of chromosome ends. The X, STR, and Y′ elements in each subtelomeric regions are marked with black, grey and white boxes, respectively. The TG_{1-3} telomeric sequences are marked with arrow tips. The XhoI digestion sites in telomere regions are indicated, and the numbers in kb in parenthesis indicate the sizes of DNA fragments recognized by the TG_{1-3} probe in the Southern blot analysis.

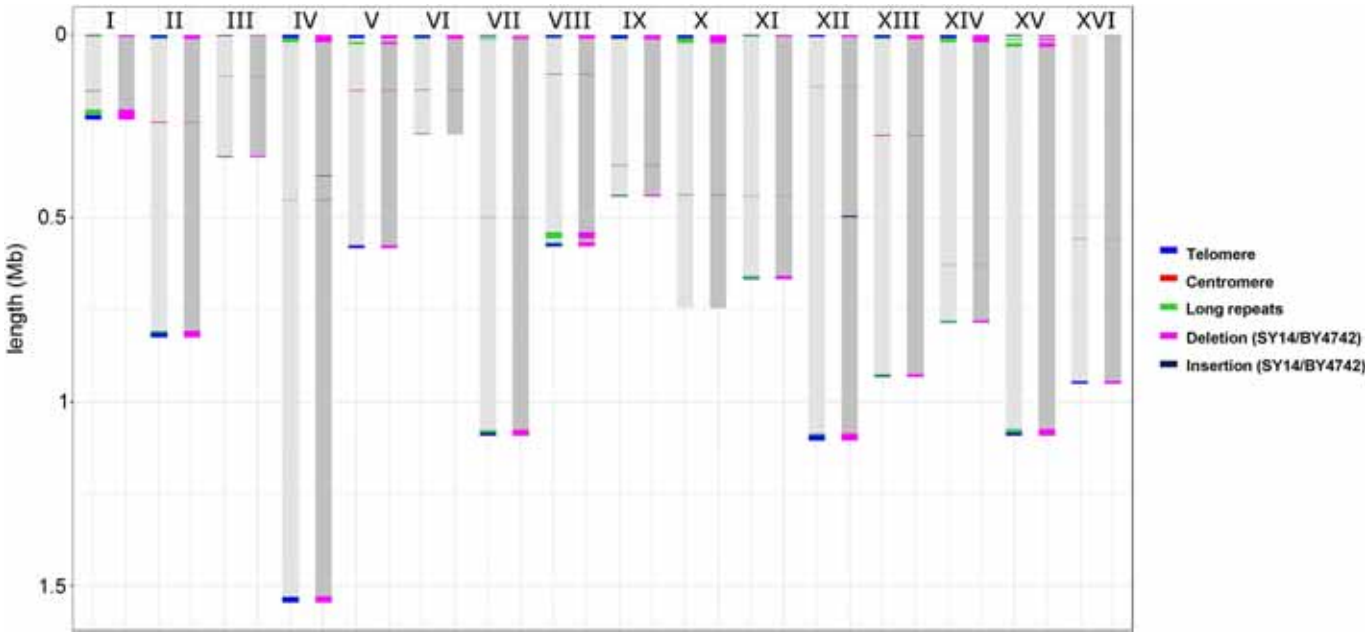

Extended Data Fig. 2 | De novo sequence comparison of BY4742 (light grey) and SY14 (dark grey) genomes. The chromosomes are labelled with Roman numerals of the yeast reference genome. The telomeres (blue), centromeres (red) and telomere-associated repeats (green) that were cut by experimental design are shown in BY4742 chromosomes. Sequence deletions and insertions identified by genomic comparison between BY4742 and SY14 are highlighted in purple and black, respectively, in SY14 chromosomes.

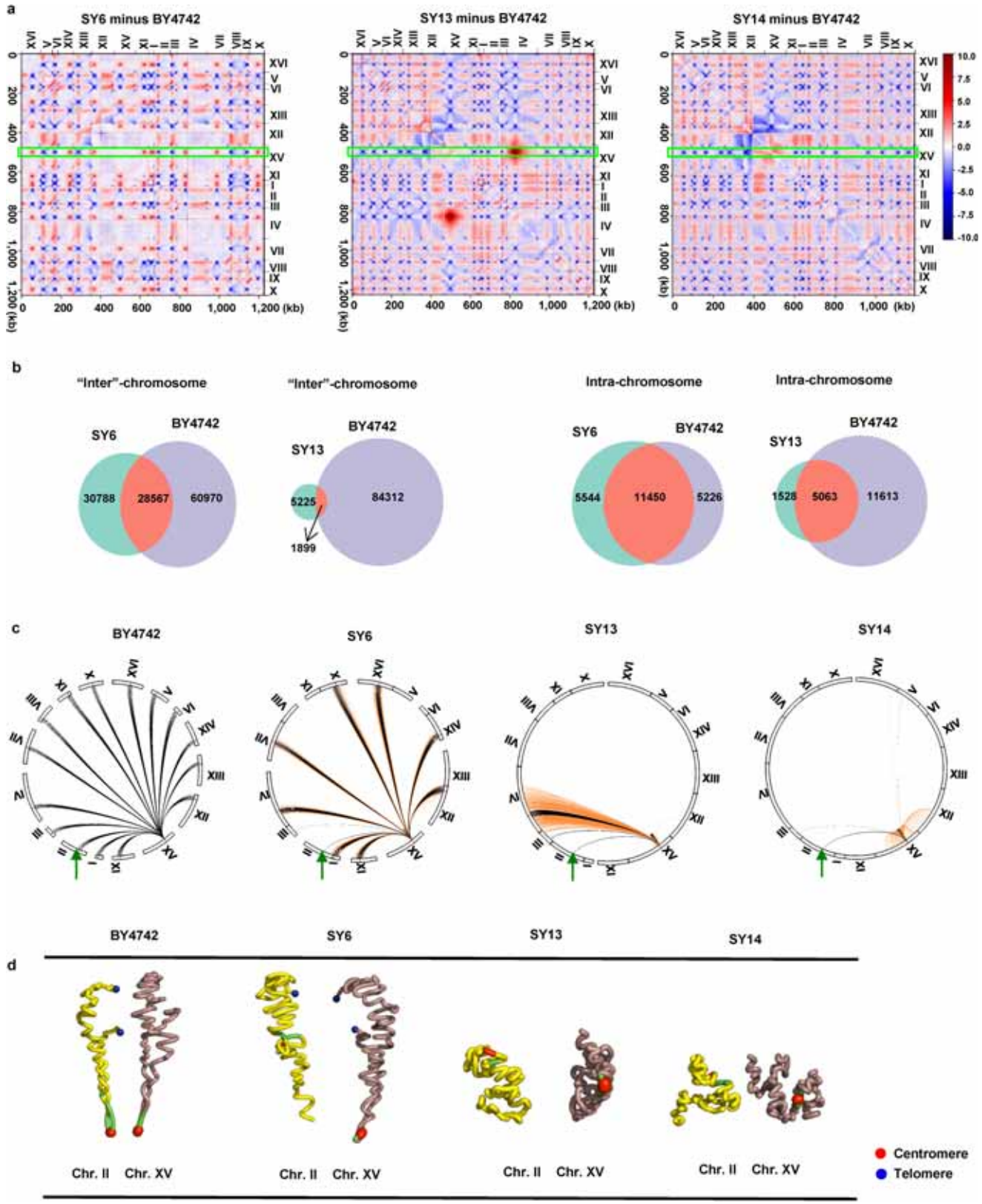

Extended Data Fig. 3 | Comparison of the chromosomal interactions of SY6, SY13 and SY14 cells with those of BY4742 cells. a, *Z*-score difference heatmaps. Bin length, 10 kb; red and blue show increased and decreased chromatin interactions, respectively. Green box highlights the interactions of the chromosome XV centromere with other chromosomes. **b**, Venn diagram of the number of significant ($P < 0.01$, $q < 0.01$) 'inter'- and intra-chromosomal interactions (referring to their locations in the BY4742 genome). **c**, Strong chromosomal interactions of chromosome XV centromere regions in the BY4742, SY6, SY13 and SY14 genomes. The red bars indicate the centromeres and their flanking regions of 50 MboI restriction sites. Each arc throughout the chromosome XV centromere area represents one strong interaction. In SY6, SY13 and SY14, the reserved interactions are marked with black arcs and new interactions are marked with orange arcs. The green arrowheads mark the ten residual interactions near the centromere regions found in all four strains. **d**, 3D structures of chromosomes XV and II in SY6, SY13 and SY14 cells compared to those in BY4742 cells. The locations of the 10 residual interactions on Chr. XV and II are marked green.

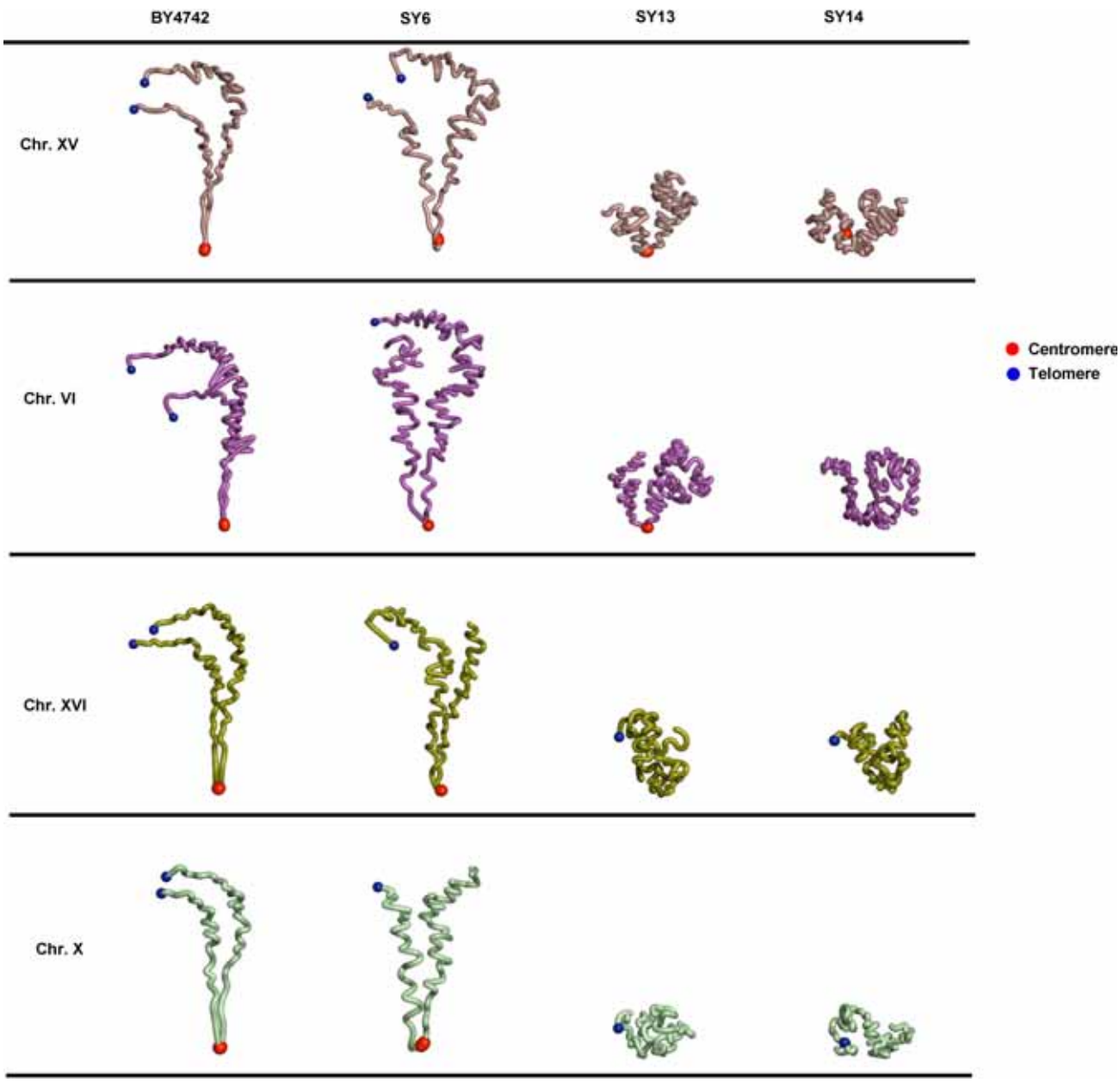

Extended Data Fig. 4 | 3D structures of single chromosomes. Chromosome structures in SY6, SY13 and SY14 cells are compared to those in BY4742 cells.

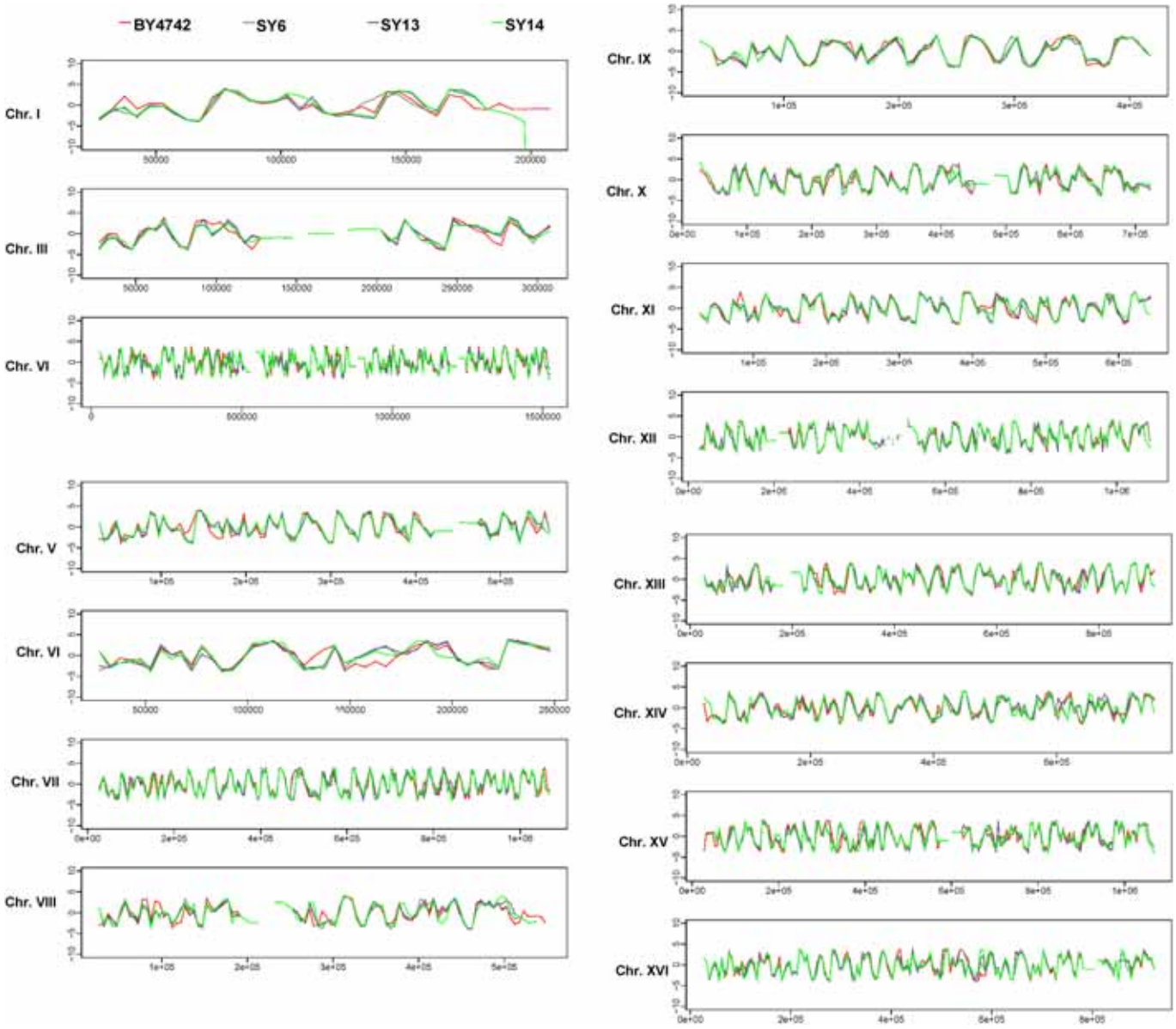

Extended Data Fig. 5 | Directional preference plots of SY6, SY13, and SY14 cells compared to BY4742 cells. Red, BY4742; moss green, SY6; purple, SY13; bright green, SY14. The *y*-axis denotes the *t*-test value between the upstream and downstream interactions of each bin. A positive *t*-value indicates that a bin has more downstream interactions, as described previously[16].

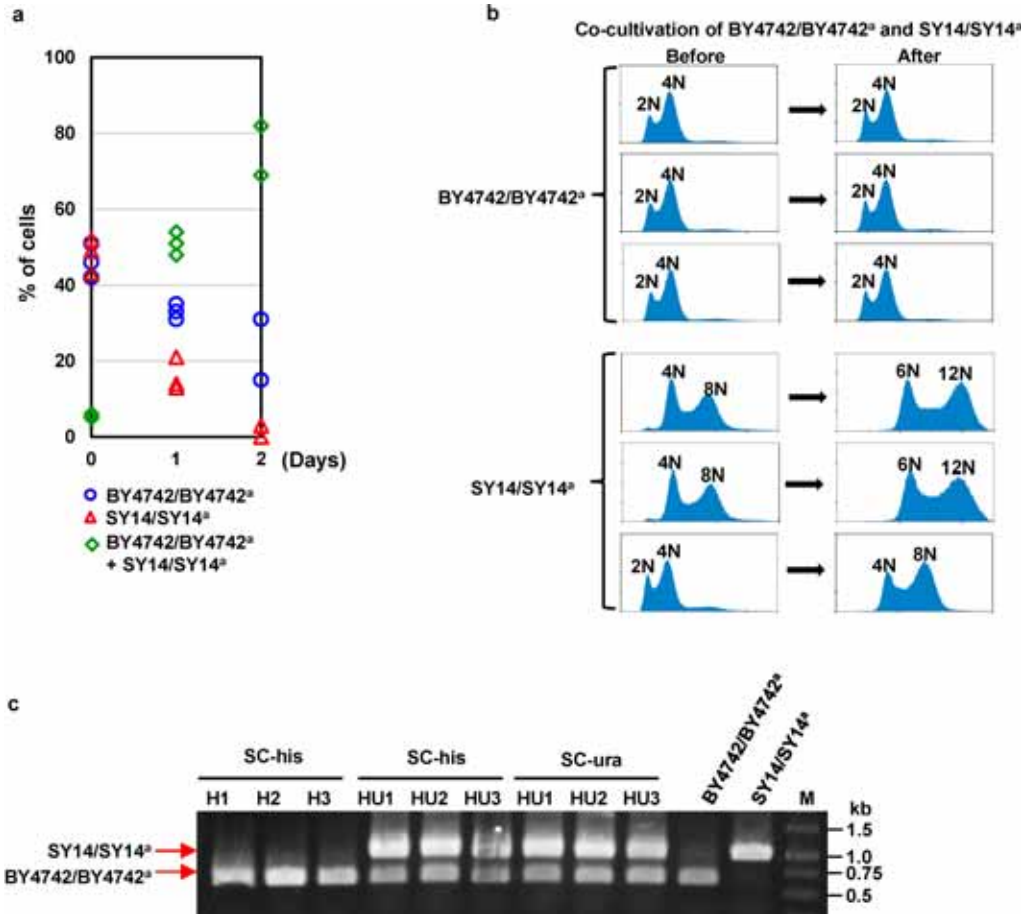

Extended Data Fig. 6 | Growth competition between SY14/SY14ª and BY4742/BY4742ª diploid cells. a, Blue circles represent BY4742/BY4742ª (with *HIS3* marker) cells that could grow only on SC-His plates; pink triangles represent SY14/SY14ª (with *URA3* marker) cells that could grow only on SC-Ura plates; green diamonds represent 'fusion' cells of BY4742/BY4742ª and SY14/SY14ª that could grow on both SC-His and SC-Ura plates. Data from three biological replicates are presented. **b**, FACS analysis of DNA content of BY4742/BY4742ª and SY14/SY14ª diploid cells before and after co-culture. Data are representative of two independent experiments. **c**, PCR verification of genomes from BY4742/BY4742ª and SY14/SY14ª diploid cells. H1–H3: colonies grown only on SC-His plates; HU1–3: colonies grown on both SC-His and SC-Ura plates. The BY4742/BY4742ª and SY14/SY14ª diploid cells before co-cultivation were used as control. Two pairs of primers, specific for genomes of BY4742/BY4742ª and SY14/SY14ª, were used. Data shown are representative images of two independent experiments.

Extended Data Table 1 | Details of the creation of a single chromosome yeast

Strain	Chromosomes to fuse (chr. length in kb)	Newly fused chromosome (+) (chr. length in kb)	Newly deleted chromosome regions (RTel: right arm telomere sequence; LTel: left arm tel sequence) (Cen: centromere sequence; RS: repetitive sequence)	No. of transformants for chromosome fusion	Positive rate of chromosome fusion
SY0	VII (1090), VIII (560)	VII+VIII (1609)	VII: 5545-9584 (RS6), 1076068-1090940 (RTel, RS3); VIII: 524501-541100 (RS1), 1-8217 (LTel), 105447-106013 (Cen) V: 18067-23447 (RS11); XV: 10454-13126 (RS9), 21791-30776 (RS10,14);	100	1/3
SY1	XIII (920), XII (1080+1500)	XIII+XII (1980+1500)	XIII: 917281-924431 (RTel, RS7), 268013-268803 (Cen); XII: 1-14474 (LTel)	26	1/3
SY2	I (230), II (810)	I+II (1006)	I: 203183-230218 (RTel, RS1,2); II: 1-9089 (LTel), 237784-238794 (Cen)	11	2/3
SY3	VI (270), XIV (780)	VI+XIV (1036)	VI: 269616-270161 (RTel), 148460-148774 (Cen); XIV: 1-17790 (LTel, RS4)	100	2/3
SY4	XVI (950), V (580)	XVI+V (1505)	XVI: 941976-948066 (RTel); V: 1-8079 (LTel), 151829-152588 (Cen)	143	4/8
SY5	IX (440), X (750)	IX+X (1160)	IX:436361-439888 (RTel), 355607-356006 (Cen); X:1-21750 (LTel, RS9,10,15)	94	1/4
SY6	III (320), IV (1530)	III+IV (1826)	III:313621-316620 (RTel), 114297-114969 (Cen); IV:1-19188 (LTel, RS12)	49	2/4
SY7	XVI-V (1505), VI-XIV (1036)	XVI-V+VI-XIV (2523)	V:569325-576874 (RTel); VI:1-8380 (LTel); XIV:628734-629219 (Cen)	130	1/5
SY8	XV (1090), XI (670)	XV+XI (1725)	XV:1073966-1091291 (RTel, RS8,7); XI: 439551-440264 (Cen), 1-3182 (LTel)	84	3/3
SY9	VII-VIII (1609), IX-X (1160)	VII-VIII+IX-X (2747)	VIII:552000-562643 (RTel); IX:1-11214 (LTel); X:436229-436425 (Cen)	30	2/5
SY10	I-II (1006), III-IV (1826)	I-II+III-IV (2821)	I:151470-151745 (Cen); II:809896-813184 (RTel); III:1-1500 (LTel)	5	2/4
SY11	XIII-XII (1980+1500), XV-XI (1725)	XIII-XII+XV-XI (3682+1500)	XII:1059256-1078177 (RTel, RS13), 150705-150969 (Cen); XV:1-3709 (LTel)	100	3/5
SY12	I-II-III-IV (2821), VII-VIII-X-X (2747)	I-II-III-IV+VII-VIII-IX-X (5558)	IV:1522800-1531933 (RTel); VII:1-1240 (LTel), 496756-497069 (Cen)	100	2/4
SY13	XVI-V-VI-XIV (2523), XIII-XII-XV-XI (3682+1500)	XVI-V-VI-XIV+XIII-XII-XV-XI (6191+1500)	XIV:779113-784333 (RTel); XVI:555957-556549 (Cen); XIII:1-9319 (LTel)	17	4/4
SY14	XVI-V-VI-XIV-XIII-XII-XV-XI (6191+1500), I-II-III-IV-VII-VIII-IX-X (5558)	XVI-V-VI-XIV-XIII-XII-XV-XI+I-II-III-IV-VII-VIII-IX-X (11737+1500)	IV:449389-449890 (Cen); XI:658549-666816 (RTel, RS5); I:1-3294 (LTel)	26	3/5

The 'Strain' column lists the strain names, and the number in parentheses indicates the size of the native or fused chromosome in kilobase (kb). An orange plus indicates a fusion event; a dash between two chromosomes means that the fusion already occurred. 'Newly deleted chromosome regions' marks the deleted regions in the corresponding chromosomes; Rtel and Ltel in blue indicate the right arm and left arm of the corresponding telomere sequences, respectively; Cen in red indicates the corresponding centromere sequence; and RS represents repetitive sequences deleted in the corresponding chromosomes. The numbers for each region are referred from the *S. cerevisiae* S288C genome (http://www.yeastgenome.org/).

Extended Data Table 2 | Information regarding long repeat sequences near chromosome ends

Types of repeat sequences	Copy number	Location on chromosomes (bp)	
		RSs to be deleted	Retained RSs
RS1	3	I: 203448-219229; VIII: 525437-539926	I:13089-27923
RS2	2	I:219230-229411	VIII: 539927-543610 ; 549638- 556001
RS3	2	VII: 1076381-1083886	II: 805133-812631
RS4	2	XIV: 7429-15942	VI: 5531-14039
RS5	2	XI: 658572-665429	III: 4327-11225
RS6	2	VII: 6223-9584	IX: 430983-434367
RS7	3	XIII: 917474-923540; XV: 1078061-1083736	XVI: 7409-13083
RS8	2	XV: 1073988-1078544	XVI: 12601-17099
RS9	3	XV: 11053-13126; X: 8269-10330	IX: 8286-10347
RS10	3	XV:22397-27006; X: 16639-21229	IX:16656-21250
RS11	2	V: 18751-23447	XIV: 772693-777126
RS12	2	IV: 905-18681	X: 727164-744901
RS13	2	XII: 1059296-1064280	III: 303903-308316
RS14	2	XV: 27007-30776	IX: 21251-25254
RS15	2	X:10331-16638	IX: 10348-16655

This Table lists 15 types of long (>2 kb) repeat sequences near telomeres, which have two or three copies. Only one copy of each long repeat sequence was retained, and the redundant copies were deleted in the SY14 strain. During the generation of the SY14 strain, six long repeats marked in red (that is, VII: 6223–9584 (RS6), VIII: 525437–539926 (RS1), V: 18751–23447 (RS11), XV: 11053–13126 (RS9), XV: 22397–27006 (RS10), and XV: 27007–30776 (RS14)), which are distal to telomeres, were deleted by two rounds of CRISPR–Cas9-mediated PCR targeting. The remaining 13 long repeats were deleted during chromosomal end-to-end fusions.

Extended Data Table 3 | SNPs and indels confirmed by re-sequencing

a

Ref-Chromosome	Ref-Loci	Ref base	Illumina sequencing		Sanger sequencing		Affected Gene	Variation Loci in Gene	Ref Codon	Variation Codon	Variation Type	Mutation in functional domain? (Y/N)	Null gene phenotypes
			WT	SY14	WT	SY14							
II	9136#	G	G	A	G	A	–	–	–	–	–	–	–
III	151645	G	G	A	G	A	–	–	–	–	–	–	–
X	517916	G	G	T	G	T	–	–	–	–	–	–	–
XV	161691	C	C	G	C	G	–	–	–	–	–	–	–
IX	145512	G	G	T	G	T	Nup159	3198	CTC->L	CTA->L	synonymous	–	–
II	447712	A	A	T	A	T	Sif2	4	AGT->S	TGT->C	non-synonymous	N	–
VII	775929	C	C	A	C	A	Skn1	737	GCT->A	GAT->D	non-synonymous	N	–
XV	454309	C	C	A	C	A	Vps5	542	ACA->T	AAA->K	non-synonymous	N	–
X	148553	G	G	A	G	A	Yak1	1838	TCT->S	TTT->F	non-synonymous	Y. Mutation within kinase domain	Null mutant grows slowly, has increased fitness and lifespan, is sensitive to DNA damage.
XI	594128	C	C	A	C	A	Nup133	1304	TCT->S	TAT->Y	non-synonymous	Y. Mutation within WD40/YVTN repeat-like-containing domain	Null mutant has abnormally elongated bud morphology, decreased cell death, abnormal chemical compound accumulation
XIV	225122	A	A	G	A	G	Sqs1	1978	TGG->W	CGG->R	non-synonymous	Y. Mutation within R3H domain	Null mutant has decreased or increased competitive fitness depend on the growth conditions.

b

Ref-Chromosome	Ref-Loci	Ref base	ALTbase	Ref len	ALT len	Illumina sequencing		Sanger sequencing		Affected Gene	Variation Loci in Gene	Mutation in functional domain? (Y/N)	Null gene phenotypes
						WT	SY14	WT	SY14				
III	114269*	TCCCC	TCCC	5	4	0	-1	0	-1	--	--	--	--
IV	450188#	GTATATATAT ATATATATAT ATAT	GTATATATAT ATATATATAT	24	20	0	-4	0	-4	--	--	--	--
VIII	524500*	T	TA	1	2	0	1	0	1	--	--	--	--
XIII	9319*	CTTT	CTTTT	4	5	0	1	0	1	--	--	--	--
XIV	17812*	TC	T	2	1	0	-1	0	-1	--	--	--	--
XVI	941970*	TG	T	2	1	0	-1	0	-1	--	--	--	--
XV	1037517	CAATAATAA TAATAATAAT AATAATAAT AATAATA	CAATAATAA TAATAATAAT AATAATAAT AATAATAAT A	35	38	0	3	0	3	Nud1p	684	N	--

#: errors located within recombination regions during chromosome fusions, but not located within primer binding sites.
*: errors located within primer binding sites.

a, SNPs. **b**, Indels.

Extended Data Table 4 | Differentially expressed genes in SY14 compared to BY4742 cells

geneID	GeneSymbol	Expression						log_2FC	Pvalue	FDR	Notes
		SY14-1	SY14-2	SY14-3	WT-1	WT-2	WT-3				
Telomere adjacent genes (<10 kb distance)											
855848	ERR2	0.04	0	0.04	2.08	1.52	2.05	-7.55	7.67E-13	6.78E-11	Chr XVI-L.
855849	HSP32	0	0.1	0	2.86	2.6	2.57	-6.83	2.83E-09	2.03E-07	Chr XVI-L.
855850	FEX2	1.11	4.51	2.73	21.54	21.83	23.7	-3.03	1.64E-12	1.38E-10	Fourth gene near XVI-L.
855852	YPL277C	1.97	2.82	2.09	7.11	5.57	8.61	-1.66	0.000071	0.004003	Sixth gene near XVI-L.
853625	MPH3	3.79	7.58	7.24	19.12	18.21	19.61	-1.65	2.78E-05	0.001666	Second gene near X-R.
854634	VTH1	25.96	23.78	29.85	8.71	8.08	11.03	1.47	0.000126	0.006776	Second gene near IX-L, first gene was deleted in SY14.
851230	SEO1	6.79	7.37	7.27	2.72	2.02	2.69	1.49	0.000254	0.013032	Third gene near I-L, the first two genes were deleted in SY14.
854002	YOL162W	25.86	21.03	21.94	10.17	6.31	5.28	1.64	9.25E-05	0.005119	Fourth gene near XV-L.
854001	YOL163W	42.33	35.02	31.7	14.94	7.6	8.11	1.82	1.53E-05	0.000936	Third gene near XV-L.
850486	THI5	4.61	5.13	4.56	1.51	0.14	1.93	1.93	3.53E-05	0.002072	Fifth gene near VI-L, first gene was deleted in SY14.
853207	MAL11	59.06	56.38	56.36	8.7	9.65	6.49	2.75	1.04E-11	8.32E-10	Fourth gene near VII-R,first three genes were deleted in SY14.
850618	YFR057W	22.58	20.31	18.16	3.13	1.46	0.96	3.40	1.64E-10	1.2E-08	First gene near VI-R.
Stress response											
852364	HSP26	60.43	56.15	60.09	24.96	18.59	20.85	1.44	0.000263	0.013364	Small heat shock protein (sHSP) with chaperone activity.
854744	RNR3	15.67	14.26	15.89	6.2	4.95	5.09	1.46	0.000184	0.009714	Minor isoform of large subunit of ribonucleotide-diphosphate reductase;regulated by DNA replication and DNA damage checkpoint pathways. Induced by DNA damage and replication stress.
853326	NCA3	85.44	90.16	83.51	32.42	31	28.38	1.47	0.000148	0.007853	Protein involved in mitochondrion organization; Induced by the SLN1-SKN7 osmotic stress signaling pathway.
850331	HBN1	30.17	22.64	28.11	10.71	6.16	8.97	1.63	9.49E-05	0.005147	Similar to bacterial nitroreductases; protein abundance increases in response to DNA replication stress.
855932	OYE3	8.01	5.63	9.95	1.71	2.57	2.83	1.69	7.08E-05	0.004003	Conserved NADPH oxidoreductase containing flavin mononucleotide (FMN),has potential roles in oxidative stress response and programmed cell death.
854944	HUG1	479.95	1084.46	860.2	381.3	251.63	167.35	1.82	0.00048	0.023808	Ribonucleotide reductase inhibitor; transcription is induced by genotoxic stress and by activation of the Rad53p pathway; protein abundance increases in response to DNA replication stress.
850532	HSP12	211.2	223.37	183.79	62.8	54.47	46.85	1.98	1.56E-06	0.000102	Plasma membrane protein involved in maintaining membrane organization; involved in maintaining organization during stress conditions; induced by heat shock, oxidative stress, osmostress,; protein abundance increased in response to DNA replication stress.
855132	YKU80	12.19	12.28	12.7	0	0.06	0.1	7.65	1.06E-33	1.97E-31	Subunit of telomeric Ku complex (Yku70p-Yku80p); involved in telomere length maintenance, structure and telomere position effect; relocates to sites of double-strand cleavage to promote nonhomologous end joining during DSB repair.
Others											
9164931	RDN37-1	82.96	93.16	86.11	13.39	13.71	16.74	2.54	1.53E-10	1.13E-08	35S ribosomal RNA (35S rRNA) transcript.
854565	FIT3	489.5	230.81	526.59	265.15	96.71	154.28	1.25	0.00102	0.049686	Mannoprotein that is incorporated into the cell wall.
852298	YBR012W-A	20.41	15.07	15.39	5.28	2.1	5.84	1.91	2.22E-06	0.000143	Retrotransposon TYA Gag gene.
854004	YOL160W	15.64	15.33	26.41	1.1	3.52	1.28	3.23	9.57E-07	6.39E-05	Putative protein of unknown function; conserved across *S. cerevisiae* strains.
851850	YDR261W-A	0.24	0	0	1.2	1.94	0	-3.57	3.33E-06	0.000213	Transposable_element_gene.
850849	TAR1	12.98	0	0.08	25.05	66.46	0	-2.88	3.81E-08	2.6E-06	Transcript Antisense to Ribosomal RNA. Protein potentially involved in regulation of respiratory metabolism.
854860	YIR042C	10.6	10.01	8.16	53.09	44.8	51.94	-2.40	5.57E-09	3.95E-07	Second gene near IX-R, first gene deleted in SY14.
853869	MET14	40.28	38.8	41.33	127.39	96.51	128.82	-1.56	5.97E-05	0.00343	First gene near centromere.

Sample size $n = 3$. Exact negative binomial two-sided test was used to generate P values. Benjamini and Hochberg's algorithm was used to control the FDR.

Corresponding author(s): Zhongjun Qin, Xiaoli Xue, Jin-Qiu Zhou, Guoping Zhao

Reporting Summary

Nature Research wishes to improve the reproducibility of the work that we publish. This form provides structure for consistency and transparency in reporting. For further information on Nature Research policies, see Authors & Referees and the Editorial Policy Checklist.

Statistical parameters

When statistical analyses are reported, confirm that the following items are present in the relevant location (e.g. figure legend, table legend, main text, or Methods section).

n/a	Confirmed	
☐	☒	The exact sample size (*n*) for each experimental group/condition, given as a discrete number and unit of measurement
☐	☒	An indication of whether measurements were taken from distinct samples or whether the same sample was measured repeatedly
☐	☒	The statistical test(s) used AND whether they are one- or two-sided *Only common tests should be described solely by name; describe more complex techniques in the Methods section.*
☐	☒	A description of all covariates tested
☐	☒	A description of any assumptions or corrections, such as tests of normality and adjustment for multiple comparisons
☐	☒	A full description of the statistics including central tendency (e.g. means) or other basic estimates (e.g. regression coefficient) AND variation (e.g. standard deviation) or associated estimates of uncertainty (e.g. confidence intervals)
☐	☒	For null hypothesis testing, the test statistic (e.g. *F*, *t*, *r*) with confidence intervals, effect sizes, degrees of freedom and *P* value noted *Give P values as exact values whenever suitable.*
☐	☒	For Bayesian analysis, information on the choice of priors and Markov chain Monte Carlo settings
☐	☒	For hierarchical and complex designs, identification of the appropriate level for tests and full reporting of outcomes
☐	☒	Estimates of effect sizes (e.g. Cohen's *d*, Pearson's *r*), indicating how they were calculated
☐	☒	Clearly defined error bars *State explicitly what error bars represent (e.g. SD, SE, CI)*

Our web collection on statistics for biologists may be useful.

Software and code

Policy information about availability of computer code

Data collection	No software was used.
Data analysis	SMRT analysis package v4.0 (https://github.com/PacificBiosciences/SMRT-Link); CANU; (version 1.5); pbalign (https://github.com/PacificBiosciences/pbalign, version 0.3.1, algorithm: blasr, hitPolicy: randombest, algorithmOptions: --bestn 1 --nCandidates 1 --bam, maxDivergence 15.0, minAccuracy 85.0) and arrow (https://github.com/PacificBiosciences/GenomicConsensus, version 2.2.0, minCoverage 15); minimap (version 0.2-r124-dirty) and miniasm (version 0.2-r137-dirty); minimus2 (https://github.com/sanger-pathogens/circlator/wiki/Minimus2-circularization-pipeline, AMOS, version 3.1.0); LAST (version 810) ; Circos(version0.67-7); ICE software package (v1f8815d0cc9e); Pastis (v0.1); Ay's Fit-Hi-C software (v1.0.1); Bowtie2 (v2.2.2); RSEM (v1.3.0); DEseq2 (v1.16.1); online services of SGD Gene Ontology Slim Mapper (http://www.yeastgenome.org/cgi-bin/GO/goSlimMapper.pl); QuASAR-Rep (from HiFive v1.5.3); Summit (version 5.2); Emily Crane's method (package cworld-dekker from https://github.com/dekkerlab/cworld-dekker/releases, v1.01); OmniLog software (version 2.3.01)

For manuscripts utilizing custom algorithms or software that are central to the research but not yet described in published literature, software must be made available to editors/reviewers upon request. We strongly encourage code deposition in a community repository (e.g. GitHub). See the Nature Research guidelines for submitting code & software for further information.

Data

Policy information about availability of data

All manuscripts must include a data availability statement. This statement should provide the following information, where applicable:

- Accession codes, unique identifiers, or web links for publicly available datasets
- A list of figures that have associated raw data
- A description of any restrictions on data availability

Genome sequencing data and the assembled genome sequences of SY14 and WT have been submitted to NCBI with a project accession number of PRJNA429985. The Hi-C sequencing data of SY6, SY13, SY14 and BY4742 have been submitted to NCBI with a project accession number of PRJNA431161. The RNA-seq data have been submitted to NCBI with a project accession number of PRJNA451522. All data can be viewed in NODE (http://www.biosino.org/node) by pasting the accession (NODEP00371807) into the text search box or through the URL: http://www.biosino.org/node/project/detail/NODEP00371807.

Field-specific reporting

Please select the best fit for your research. If you are not sure, read the appropriate sections before making your selection.

☒ Life sciences ☐ Behavioural & social sciences ☐ Ecological, evolutionary & environmental sciences

For a reference copy of the document with all sections, see nature.com/authors/policies/ReportingSummary-flat.pdf

Life sciences study design

All studies must disclose on these points even when the disclosure is negative.

Sample size	Two and three independent biological replicates were used for Hi-C analysis and RNA-seq analysis, respectively, the sample size of which is commonly used in published papers.
Data exclusions	For Hi-C analysis, only the interactions which both p-value and q-value less than 0.01 were identified as significant interactions. For RNA-seq analysis, only the fold changed more than 2 and false discovery rate (FDR) <0.001 were identified as significant differentially expressed genes.
Replication	All attempts at replication were successful.
Randomization	For the creating of the single chromosome yeast, the order of chromosome fusions was randomly chosen.
Blinding	For the creating of the single chromosome yeast, the investigators were blinded to the order of chromosome fusions because there were no any reported information for guidance.

Reporting for specific materials, systems and methods

Materials & experimental systems

n/a	Involved in the study
☒	☐ Unique biological materials
☐	☒ Antibodies
☐	☒ Eukaryotic cell lines
☒	☐ Palaeontology
☒	☐ Animals and other organisms
☒	☐ Human research participants

Methods

n/a	Involved in the study
☒	☐ ChIP-seq
☐	☒ Flow cytometry
☒	☐ MRI-based neuroimaging

Antibodies

Antibodies used	Antibodies used in Immunofluorescences Anti-Myc: Sigma, catalog no. CG1965, rabbit, polyclonal, 1:200 dilution, primary antibody for detection of the 13Myc-tagged telomere binding protein Sir2. Anti-Nop1: Santa Cruz, catalog no. SC-71715, mouse, Monoclonal, 1:200 dilution, primary antibody for detection of the nucleolus protein Nop1.

	Anti-rabbit IgG: Jackson ImmunoResearch, catalog no. 711-165-152, donkey, 1:1000 dilution, Cy3-conjugated secondary antibody for detection of anti-Myc. Anti-mouse IgG: Molecular probes, catalog no. A21202, donkey, 1:1000 dilution, Alexa 488-conjugated secondary antibody for detection of anti-Nop1.
Validation	None as all antibodies were directly purchased from companies.

Eukaryotic cell lines

Policy information about cell lines

Cell line source(s)	Saccharomyces cerevisiae strain BY4742 were bought from Euroscarf.
Authentication	None as directly purchased from Euroscarf.
Mycoplasma contamination	The Saccharomyces cerevisiae strain BY4742 were not tested for mycoplasma contamination.
Commonly misidentified lines (See ICLAC register)	No commonly misidentified cell lines were used.

Flow Cytometry

Plots

Confirm that:

☒ The axis labels state the marker and fluorochrome used (e.g. CD4-FITC).

☒ The axis scales are clearly visible. Include numbers along axes only for bottom left plot of group (a 'group' is an analysis of identical markers).

☒ All plots are contour plots with outliers or pseudocolor plots.

☒ A numerical value for number of cells or percentage (with statistics) is provided.

Methodology

Sample preparation	The collected cells were washed and fixed in 70% ethanol at 4 oC overnight. Cells were then treated with RNase (20 mg/mL, Sigma) at 37 oC for 2–3 hours. Samples were stained by PicoGreen (Invitrogen), and analyzed by flow cytometry.
Instrument	Beckman MoFlo XDP
Software	Summit 5.2
Cell population abundance	Approximately, 90% of the cell populations was selected after sorting.
Gating strategy	We used the FSC to select the majority of cell populations and remove the cell debris, then FL1 for selection of cells with fluorescence.

☐ Tick this box to confirm that a figure exemplifying the gating strategy is provided in the Supplementary Information.